SURFACE ROUGHNESS MEASUREMENTS UTILIZING LONG-RANGE SURFACE-PLASMA WAVES

Dror Sarid
Optical Sciences Center
University of Arizona
Tucson, Arizona 85721

November 1984

Final Report for Period 29 November 1982 - 30 June 1984

Approved for public release;
distribution unlimited.

Prepared for
Defense Advanced Research Projects Agency
Arlington, Virginia

UNCLASSIFIED

SECURITY CLASSIFICATION OF THIS PAGE

REPORT DOCUMENTATION PAGE

1a. REPORT SECURITY CLASSIFICATION Unclassified	1b. RESTRICTIVE MARKINGS
2a. SECURITY CLASSIFICATION AUTHORITY	3. DISTRIBUTION/AVAILABILITY OF REPORT Approved for public release; distribution unlimited.
2b. DECLASSIFICATION/DOWNGRADING SCHEDULE	
4. PERFORMING ORGANIZATION REPORT NUMBER(S)	5. MONITORING ORGANIZATION REPORT NUMBER(S)
6a. NAME OF PERFORMING ORGANIZATION Optical Sciences Center 6b. OFFICE SYMBOL (If applicable)	7a. NAME OF MONITORING ORGANIZATION Naval Weapons Center
6c. ADDRESS (City, State and ZIP Code) University of Arizona Optical Sciences Center Tucson, AZ 85721	7b. ADDRESS (City, State and ZIP Code) China Lake, CA 93555
8a. NAME OF FUNDING/SPONSORING ORGANIZATION DARPA 8b. OFFICE SYMBOL (If applicable)	9. PROCUREMENT INSTRUMENT IDENTIFICATION NUMBER N60530-83-C-0089
8c. ADDRESS (City, State and ZIP Code) 1400 Wilson Blvd Arlington VA 22209	10. SOURCE OF FUNDING NOS. PROGRAM ELEMENT NO / PROJECT NO. / TASK NO. / WORK UNIT NO.
11. TITLE (Include Security Classification) Surface Roughness Measurements ...	
12. PERSONAL AUTHOR(S) Dror Sarid	
13a. TYPE OF REPORT Final Report 13b. TIME COVERED FROM 11-29-82 TO 6-30-84	14. DATE OF REPORT (Yr., Mo., Day) November 1984 15. PAGE COUNT 3 + attachments
16. SUPPLEMENTARY NOTATION	
17. COSATI CODES FIELD / GROUP / SUB GR	18. SUBJECT TERMS (Continue on reverse if necessary and identify by block number) Thin films Surface plasmon polaritons

19. ABSTRACT (Continue on reverse if necessary and identify by block number)

During the contract period we (1) performed an experiment to measure the dispersion of the long-range surface-plasmon polaritons as a function of the metal thickness along which they propagate, (2) developed a theory for the profile of the light reflected from the prism-metal structure, and (3) performed an experiment to observe this shape. Preliminary calculations (submitted in the interim report) indicate that our system is capable of measuring surface roughness of thin metal films down to several angstroms.

20. DISTRIBUTION/AVAILABILITY OF ABSTRACT UNCLASSIFIED/UNLIMITED ☐ SAME AS RPT ☐ DTIC USERS ☐	21. ABSTRACT SECURITY CLASSIFICATION Unclassified
22a. NAME OF RESPONSIBLE INDIVIDUAL	22b. TELEPHONE NUMBER (Include Area Code) 22c. OFFICE SYMBOL

DD FORM 1473, 83 APR EDITION OF 1 JAN 73 IS OBSOLETE.

Unclassified

SECURITY CLASSIFICATION OF THIS PAGE

Grant title: Surface-Roughness Measurements Utilizing Surface-Plasma Waves

Grant number: N60530-83-C-0089

Effective dates: November 29 (82) - November 29 (83).

Principal Investigator: Dror Sarid

During the contract period we (1) performed an experiment to measure the dispersion of the long-range surface-plasmon polaritons as a function of the metal thickness along which they propagate, (2) developed a theory for the profile of the light reflected from the prism-metal structure, and (3) performed an experiment to observe this shape. Preliminary calculations (submitted in the interim report) indicate that our system is capable of measuring surface roughness of thin metal films down to several angstroms.

The following pages list the personnel associated with this effort and the publications that resulted. A copy of each publication is included.

Students

Alan E. Craig, University of Arizona, Tucson Arizona 85721.

Alan earned his PhD degree in 1984. His thesis title is "Surface Plasmons on Thin Metal Films."

Grieg A. Olson, University of Arizona, Tucson Arizona 85721.

Grieg will receive his MS degree in 1984-1985. His thesis title is "Experimental Observation of the Profile of the Light Reflected from a Long-Range Surface Plasmon Polariton."

Consultants:

1. Robert T. Deck, University of Toledo, Toledo, Ohio 43606.

2. J. Merle Elson, Naval Weapons Center, China Lake, California 83555.

PUBLICATIONS

1. Dror Sarid, "Long-Range Surface-Plasma Waves on Very Thin Metal Films," Phys. Rev. Lett. 47, 1927 (1981).

2. Dror Sarid, Robert. T. Deck, Alan. E. Craig, Robert. K. Hickernell, Ralph S. Jameson, and Joseph J. Fasano, "Optical Field Enhancement by Long-Range Surface-Plasma Waves," Appl. Opt. 21, 3994 (1982).

3. Alan E. Craig, Grieg E. Olson, and Dror Sarid, "Experimental Observation of the Long-Range Surface-Plasmon Polariton," Optics Letters 8, 380 (1983).

4. Robert T. Deck, Dror Sarid, Grieg E. Olson, and J. Merle Elson, "Coupling between Finite Width Electromagnetic Beam and Long-Range Surface-Plasmon Mode," Appl. Opt. 22, 3397 (1983).

5. Dror Sarid, "Long-Range Surface-Plasmon Polaritons," in "Optics 83': A Report on Emerging Technologies," Optics News, Nov. 1983.

6. Alan E. Craig, Grieg. A. Olson, and Dror Sarid, "Novel System for Coupling to Surface-Plasmon Polaritons," Appl. Opt. (Accepted).

Long-Range Surface-Plasma Waves on Very Thin Metal Films

Dror Sarid
Optical Sciences Center, University of Arizona, Tucson, Arizona 85721
(Received 17 August 1981)

The dispersion equation of injected surface-plasma waves that propagate on thin metal films has been solved as a function of the film thickness, and splitting of the modes into two branches is observed. For one branch the imaginary part of the propagation constant goes to zero as the thickness of the metal decreases. Reflectivity calculations agree with this result, which predicts that one can obtain propagation distances that are more than 1 order of magnitude larger than observed before.

PACS numbers: 73.60.Dt

The lifetime or decay constant of a surface-plasma wave (SPW) that propagates on a metal surface is an important physical quantity because it is a strong function of the properties of the metal surface, and can therefore serve as a sensitive probe for characterizing surface conditions such as roughness and composition.[1-4] There is only one SPW mode for thick metal films, and the upper limit of its propagation range is determined by the complex refractive index of the metal and the loss introduced by the medium bounding the metal.[5]

The existence of two thermally excited SPW modes, one symmetric and one antisymmetric, that propagate on an unsupported thin metal film (the two media bounding the metal film are identical) has been discussed theoretically and verified experimentally by using electron scattering techniques.[6,7] The theory that predicted the existence of these two modes did not treat the problem of their lifetime and optical-wavelength dependence, and since the resolution and signal-to-noise ratio of the experiments were low, the linewidth of these modes could not be measured.

A comprehensive analysis of the dispersion of SPW that propagate on various combinations of thin metal films sandwiched between thin dielectric films revealed the existence and splitting of the SPW modes as the metal thickness decreases.[8,9] The theory dealt only with the dependence of the real wave vector on the real part of the frequency, and did not treat the properties of the imaginary part of the frequency, which is associated with the lifetime of the thermal SPW.

The theory of the dispersion and lifetime of thermal SPW that propagate on supported or unsupported thin metal films has been discussed by Fukui, So, and Normandin.[10] Their theoretical conclusion was that, for an unsupported metal film, there is a SPW mode that has a lifetime which increases as the thickness of the metal film decreases, while for the supported metal film such a mode does not exist.

In this Letter a different case is treated, namely that of "injected" SPW, where the frequency is a real quantity, while the wave vector is complex. It is shown that for both the supported and unsupported metal films one can excite a SPW mode having a decay constant that goes to zero as the film thickness becomes small enough, and that this mode can exist even in the visible range of the spectrum. The reflectivity at the base of a prism that is placed close to a thin metal film has also been calculated with identical results. The theory of the splitting of the SPW modes and their properties and means of excitation is discussed; this long-range mode offers a unique opportunity for probing the characteristics of metal surfaces.

The geometry of the thin metal film that is coupled to a prism, and that supports the SPW, is shown in Fig. 1, where n_0, $n_1 = n' + in''$, n_2, and n_3 are the refractive indices of the substrate, metal film, gap, and prism, respectively, and t and s are thicknesses of the metal and the gap, respectively.

The standard dispersion relation for a free TM mode ($s \gg \lambda$) that is guided by a thin dielectric, semiconductor, or metal film, is given by[11]

$$KBt = \tan^{-1}(k_{10}) + \tan^{-1}(k_{12}) + m\pi, \tag{1}$$

where $K = 2\pi/\lambda$, λ is the free-space optical wavelength, $k_{10} = \epsilon A/n_0^2 B$, and $k_{12} = \epsilon C/n_2^2 B$. Here $A^2 = \beta^2 - n_0^2$, $B^2 = n_1^2 - \beta^2$, $C^2 = \beta^2 - n_2^2$, $K\beta$ is the propagation constant of the guided wave, $\epsilon = n_1^2$, and m is the mode number. Equation (1) is an implicit complex equation in the complex variable $\beta = \beta' + i\beta''$, where β' is related to the speed of the mode by $v = c/K\beta'$, and β'' is related to the amplitude attenuation of the mode by $\alpha = K\beta''$.

A considerable simplification in the solution of Eq. (1) can be made by defining

$$k = (k_{10} - i)(k_{12} - i)/(k_{10} + i)(k_{12} + i). \tag{2}$$

From Eqs. (1) and (2) one obtains the real implicit dispersion relation with real variables

$$\tan[(B'/B'')\ln|k|] + k''/k' = 0, \tag{3}$$

where k' and k'' are the real and imaginary components of k, respectively. To solve Eq. (3), one chooses a value for β', and then searches for the value of β'' such that Eq. (3) is satisfied. Consequently, one has to use complex numbers only for the evaluation of A, B, C, and k; a simple computer routine will solve for β''. The film thickness is obtained by

$$t = -\ln|k|/2K\beta''. \tag{4}$$

All the modes we are considering here have a mode number $m = 0$. By using Eq. (1) it is possible to generate curves of the interdependence of the three variables β', β'', and t, for a given set of refractive indices. These calculations have been carried out for various combinations of parameters at optical wavelengths extending from the visible to the far infrared.

For a thick, unsupported metal film, in which the two bounding media are identical, the speed and decay constant of the SPW's on each one of the interfaces are the same. Each one of these two SPW's has an evanescent wave extending both into the dielectric medium and into the metal film. If the metal film is thick enough, the evanescent waves inside the metal that belong to the two SPW's do not overlap: As the film thickness decreases, the evanescent waves of the otherwise decoupled modes begin to overlap, and a transverse standing wave is established. The degenerate SPW mode therefore splits into one symmetrical and one antisymmetrical mode (referring to the transverse electric field distributions). These symmetric and antisymmetric modes are characterized by a range that increases and decreases, respectively, as the film thickness decreases.

For a thick, supported metal film, in which the

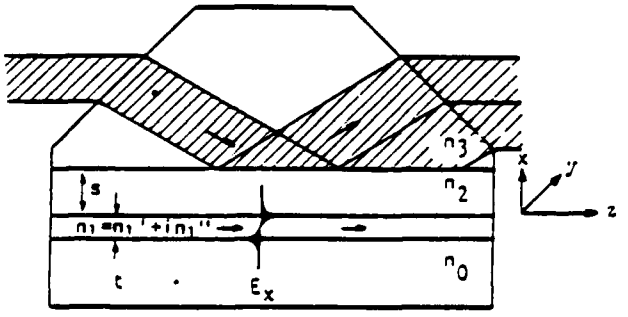

FIG. 1. The geometry of the prism to surface-plasmon wave coupler. Note the antisymmetric (transverse) electric field distribution of the long-range mode.

two bounding media are not identical, the modes that propagate on each one of the two interfaces have different speeds and decay constants and their evanescent fields inside the metal do not overlap. As the metal thickness decreases, these evanescent fields begin to overlap, and each one of these two modes splits into two branches, as in the unsupported case, one having a decreasing range and one having an increasing one. In the supported metal film case, however, extra interfering terms between the two evanescent waves inside the metal will limit the range of the antisymmetric mode if the difference between the refractive indices of the two media bounding the metal is too large.

In Fig. 2 the dependence of β' (dashed lines) and β'' (solid lines) on the metal thickness t is shown for the case of the free SPW. The parameters used are $n_0 = 1.5$, $n_1 = 0.0657 + i4$ (Ag), $n_2 = 1.55$, and $\lambda = 6328$ Å. One observes the decrease in both β' and β'' for the antisymmetric mode as t decreases. The physical validity of the results of these calculations has been verified by checking the value of the evanescent propagation constants, A and C, for each resultant β', β'', and t, to insure that the SPW is actually confined to the thin metal film. For each case the magnitude and phase of the electric and magnetic fields across the thin metal film has been calculated. The absolute value of the (unscaled) magnetic field $H_y(x)$ is shown in Fig. 3 for the metal film that is in the y-z plane with a thickness $t = 200$ Å. In (a), $\beta = 1.5507 + i0.0001615$, $A = 0.39 + i0.00064$, and $C = 0.047 + i0.0053$. Outside the film, the field is evanescent, while in the film it obtains a small dip. In (b), $\beta = 2.14 + i0.0325$, $A = 1.53 + i0.046$, and $C = 1.44 + i0.059$, and the field obtains a value of zero at about the center of the film. There are two electric fields, $E_z(x)$ and $E_x(x)$, the first being proportional to $H_y(x)$ in each one of the three regions and for the two modes. The second field is proportional to the derivative of $H_y(x)$ with respect to x in each one of the three regions, with (a) and (b) interchanged. One observes that in (a) the evanescent fields penetrate the media bounding the film much deeper than in (b). It is assumed that the only loss the SPW suffers is due to the dissipation of power inside the metal film. Since the mode in (a) has a smaller fraction of its field inside the metal than mode (b) has, it will have a larger propagation range.

In order to assess the feasibility of exciting this long-range mode, the reflectivity at the base of the prism, as shown in Fig. 1, has been calculated for the same material parameters used for the free SPW. It was found that in order to observe the extremely narrow dip in the reflectivity, which is associated with the excitation of the long-range mode, one has to scan across the angle of incidence of the input beam with a very high resolution. Since this mode has a large evanescent field, the angle for optimum excitation is close to the critical angle. As a result, small changes in the incidence angle produce

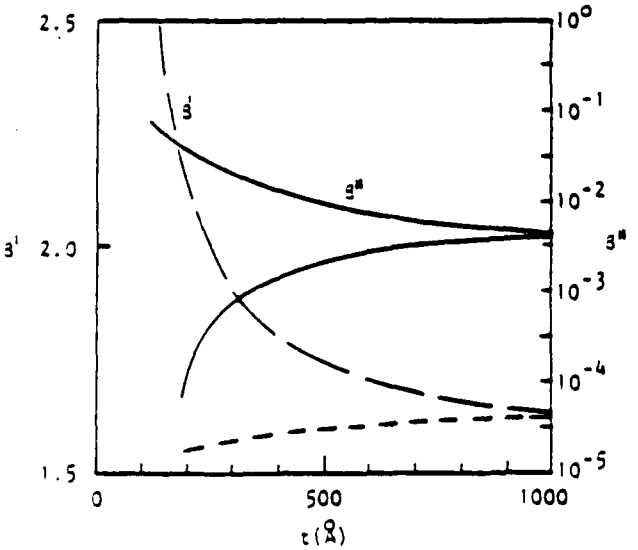

FIG. 2. The real ($K\beta'$) and imaginary ($K\beta''$) propagation constants of a surface-plasma wave propagating on a thin Ag film. Here $n_0 = 1.5$, $n_2 = 1.55$, $\lambda = 6328$ Å, and $s \gg \lambda$. Note that the decay constant $\alpha = K\beta''$ goes to zero as the metal film thickness decreases.

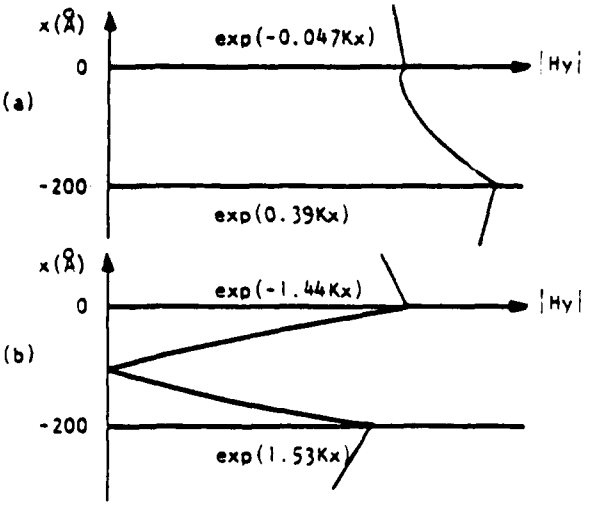

FIG. 3. The absolute value of the transverse magnetic field distribution of the (a) long-range and (b) short-range modes (not to scale.)

large changes in the penetration depth of the evanescent fields. For each angle of incidence, therefore, the gap thickness s has to be adjusted so that the proximity of the prism will have exactly the same damping effect on the otherwise freely propagating SPW. If s is too large, the excitation will be inefficient, while if s is too small, the proximity of the prism will load and wipe out the SPW.

Reflectivity calculations with use of the same parameters as in Fig. 2 yield, for a metal thickness of 200 Å, the following results: The critical angle is 32.6244°, the angle at maximum absorption is 32.6414° and the half-width angle is 0.004°. The distance which the long-range mode propagates on the 200 Å thin film until its power decays by a factor of $1/e^2$ is therefore 300 μm, which is 27 times larger than for a SPW that propagates on the surface of a thick Ag slab. Since the range of this mode is very large, its study in the case that the surfaces are randomly rough can provide useful quantitative information about roughness-induced attenuation. As a result, this mode can be used as a probe for characterizing the properties of surfaces and thin metal films. This long-range mode can also be utilized for nonlinear interactions such as second-harmonic generation where the nonlinearity is introduced by the metal itself or by the bounding media via the evanescent fields. By imbedding the thin metal film in an (optical) power-dependent refractive-index semiconductor, one obtains for the long-range SPW a power-dependent propagation-constant which can be used for bistability studies.[12]

In summary, this theory predicts that it is possible to choose material and geometrical parameters such that a long-range SPW mode could be excited on a thin metal film, the range being more than 1 order of magnitude greater than observed before. This mode can be used for the study of rough surfaces and various nonlinear interactions where a large interaction range is desirable.

Useful discussions with G. I. Stegeman and A. Craig are acknowledged. This work is supported by the Air Force Office of Scientific Research, U. S. Air Force, and the Army Research Office, U. S. Army, under Contract No. JSOP F49620-80-C-0022.

[1]A. A. Maradudin and D. L. Mills, Phys. Rev. B 11, 1392 (1975).

[2]G. J. Kovacs and G. D. Scott, Phys. Rev. B 16, 1297 (1977).

[3]J. A. Bush, D. K. Cohen, K. D. Scherkoske, and S. O. Sari, J. Opt. Soc. Am. 8, 1020 (1980).

[4]W. P. Chen and J. M. Chen, Surf. Sci. 91, 601 (1980).

[5]J. Schoenwald, E. Burstein, and J. M. Elson, Solid State Commun. 12, 185 (1973).

[6]H. Boersch, J. Geiger, A. Imbusch, and N. Niedrig, Phys. Lett. 22, 146 (1966).

[7]J. B. Swan, A. Otto, and H. Fellenzer, Phys. Status Solidi 23, 171 (1967).

[8]E. N. Economou, Phys. Rev. 82, 539 (1960).

[9]K. I. Kliewer and R. Fuchs, Phys. Rev. 53, 498 (1967).

[10]M. Fukui, V. C. Y. So, and R. Normandin, Phys. Status Solidi 91, K61 (1980).

[11]P. K. Tien and R. Ulrich, J. Opt. Soc. Am. 60, 1325 (1970).

[12]D. Sarid, Appl. Phys. Lett. 39, 889 (1981).

Optical field enhancement by long-range surface-plasma waves

Dror Sarid, Robert T. Deck, Alan E. Craig, Robert K. Hickernell, Ralph S. Jameson, and Joseph J. Fasano

Joseph Fasano is with U.S. Army, ARRADCOM, Dover, New Jersey 07801; the other authors are with University of Arizona, Optical Sciences Center, Tucson, Arizona 95721.

Received 21 May 1982.

Consider a TM polarized monochromatic wave that is incident on the base of a prism from which it is totally internally reflected. If a metallic substrate is placed in the vicinity of the prism so that the evanescent fields of the reflected light penetrate the metal, and the incident angle is appropriate, a surface-plasma wave can be excited along the metal gap. Otto[1] has analyzed this geometry and has shown both theoretically and experimentally that by measuring the reflectivity of a plane wave as a function of the angle of incidence one obtains both the speed and the range of the surface-plasma wave from the position of the minimum and the width of the Lorentzian absorption curve, respectively. In his geometry the metal thickness was much larger than the decay length of the surface-plasma field in the metal. Kretschmann[2] considered a different geometry in which a thin metal film is deposited on the bottom of the prism and a plane wave incident on the base of the prism excites a surface-plasma wave on the lower side of the metal film. The excitation in this case takes place via the optical fields that penetrate the metal. As with the Otto geometry, the excitation is possible because the speed of the surface-plasma wave is slower than the speed of the light in the prism.

Weber and Ford[3] have recently shown that the fields accompanying the surface-plasma wave are larger than those associated with total internal reflection in the absence of surface-plasma waves. In their theory they assume a general coupling mechanism that is 100% efficient and equate the optical power density injected by the coupler under steady state conditions to the power dissipated by the surface-plasma wave.

They show that the excitation of a surface-plasma wave at an optical frequency can give rise to an enhancement of the optical electric fields at a silver metal surface by a factor as large as 60. Their theory, however, is approximate because in calculating the enhanced fields they use the free surface-plasma fields instead of the true fields in the presence of the excitation medium (a prism or a grating, for example.)

In this Letter we wish to show theoretically that (1) it is possible to obtain an exact solution to the field enhancement for both the Otto and the Kretschmann geometries and (2) our new geometry[4] makes it possible to obtain field enhancements that are as much as an order of magnitude larger than those obtainable with the two other geometries.

The three prism-coupling geometries are shown in Fig. 1, where I and III correspond to the Otto and Kretschmann geometries, respectively, and II to our geometry. In each case

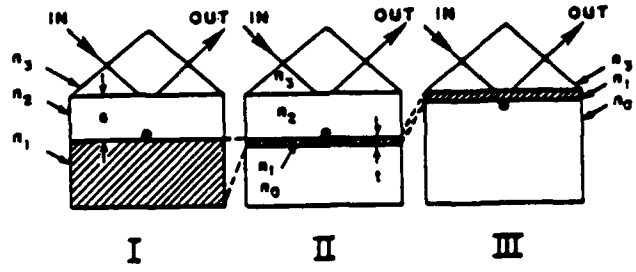

Fig. 1. Three prism-coupling geometries for exciting a surface-plasma wave: I, III, and II correspond to the Otto, Kretschmann, and our geometries, respectively.

t denotes the metal thickness, and the black dot in each diagram indicates the point where the optical fields are evaluated. In geometries I and II the evanescent fields created at the prism surface need to penetrate an intermediate medium separating the prism and the metal film. The exponential decay of the field amplitude in this medium is expressed by the factor $h = \exp(-KCS)$, where $K = 2\pi/\lambda$, λ is the optical wavelength in free space, S and n_2 are the thickness and refractive index of the gap, $C^2 = \beta^2 - n_2^2$, and $K\beta$ is the propagation constant of the surface-plasma wave which has only a real part for the plane wave approximation. In this work we assume a varying thickness S so that $h = 0.1$ for any given angle. The reason for this choice is that under these conditions the reflectivity obtains its minimum value for the appropriate angle for most of the cases we consider. It can be seen that geometry II merges into the Otto geometry for t sufficiently large and $h < 1$ and into the Kretschmann geometry for t sufficiently small and $h = 1$. For geometry II to be maximally effective, the refractive indices of the media bounding the metal film on either side need to be approximately the same.

Now in the general case of a stratified medium characterized by complex dielectric constants the reflectivity of a TM polarized monochromatic plane wave at the surface of the medium and the fields excited in each of the media can be computed by standard techniques.[5] For the plane wave assumption to be applicable to our geometry it is necessary that the range of the surface-plasma wave be appreciably smaller than the width of the incident optical beam. In the visible range of the spectrum, where the latter range is <1 mm, this requirement is easily satisfied, and the simple plane wave calculations yield accurate results for all three geometries.

To demonstrate the field enhancement obtainable with our geometry we choose parameters appropriate to the case of a silver metal film having a dielectric constant given by $-16 + i0.52$ at a wavelength of 632.8 nm, bounded by two dielectric media having a refractive index of 1.5. Our prism is assumed to be rutile with a refractive index of 2.875. Figure 2 shows the amplitude reflectivity at the base of the prism for three metal film thicknesses: $t = 2000$, 70, and 50 nm with $h = 0.1$. Note how the single Lorentzian absorption curve associated with the thick metal film splits into two Lorentzians as the film thickness decreases. The splitting is a direct result of the lifting of the degeneracy in the propagation constants of the

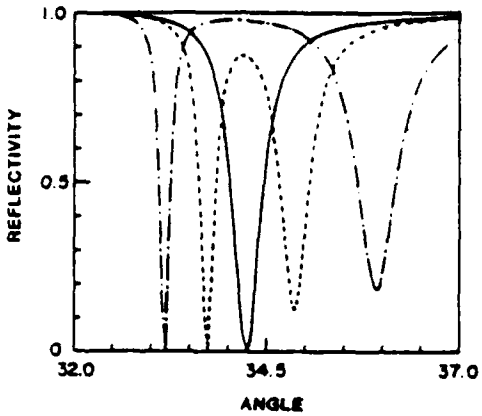

Fig. 2. Reflectivity as a function of the incident angle inside the prism for our geometry where $n_0 = n_2$. (—), (- - -), and (— - -) are for t = 2000, 70, and 50 nm, respectively. Note the splitting of the single Lorentzian into two Lorentzians as the metal film thickness decreases. The wide and the narrow Lorentzians correspond to the short-range and long-range surface-plasma waves, respectively.

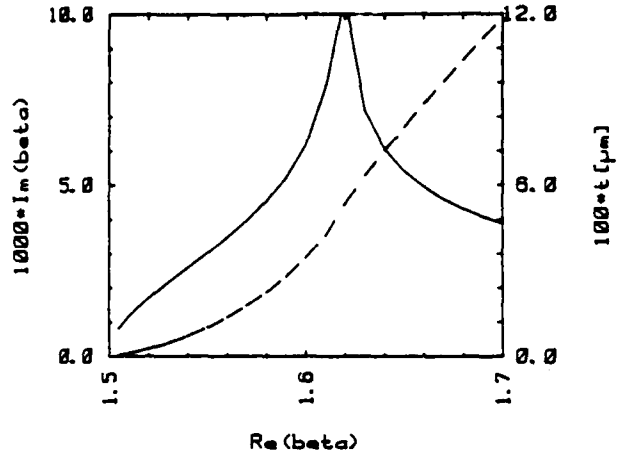

Fig. 3. Dispersion curves of the free surface-plasma waves: Im(β) (dashed line) and t (continuous line) as a function of Re(β). Note the divergence of t for Re(β) that corresponds to the thick metal case, and the two values of Re(β) and Im(β) for each t for the thinner metal case.

two independent surface-plasma waves propagating on each surface of the thick metal. Once the metal film thickness becomes small enough, the fields of these two surface-plasma waves inside the metal overlap, and the degeneracy is lifted. For such a thickness, one long-range and one short-range surface-plasma wave can be excited as a single eigenmode that satisfies all the boundary conditions simultaneously.[4] One observes that the Lorentzian width at half maximum for the short-range and for the long-range mode increases and decreases, respectively. The width consists of two contributions, one from the power dissipation in the metal film and one from the prism loading. This analysis differs from that of Weber and Ford, because it takes into account the important fact that any efficient means of excitation has in principle to interfere with the excited system which can no longer be considered to exist as a free one. In this respect our analysis is more accurate.

Figure 3 shows the dispersion curves of the free surface-plasma waves in the absence of the prism loading. The dashed and continuous curves show, respectively, the imaginary part of β and the metal thickness t as a function of the

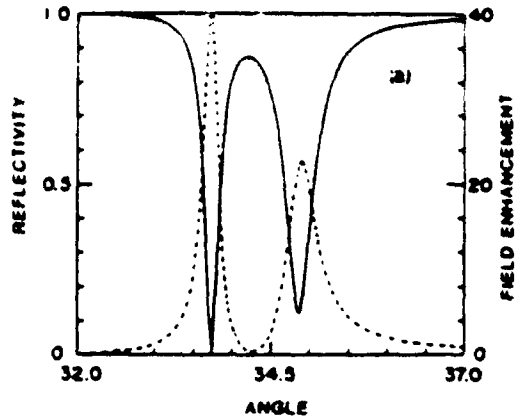

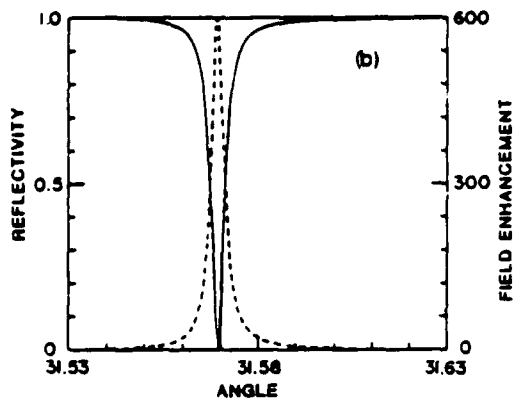

Fig. 4(a) Reflectivity (continuous line) as a function of the incident angle and the ratio of the absolute square of the magnetic fields at the metal surface and inside the prism (dashed line) for t = 70 nm. (b) Same as (a) but with t = 10 nm. Note the enhancement of the optical fields relative to the thick metal case.

real part of β. One observes the divergence of t for a value of β which corresponds to the degenerate case discussed before. For smaller values of t one obtains two values for both the real and imaginary parts of the propagation constant, each pair of real and imaginary values corresponding to either the short-range or the long-range mode. In the presence of the prism loading (with h = 0.1) the Lorentzian width shown in Fig. 2 is approximately a factor of 2 larger than the one computed from Im(β) in Fig. 3. The chosen value of h, therefore, has the effect of roughly equalizing the plasma-wave losses associated with reradiation and dissipation in the metal.

In Figs. 4(a) and (b) we show the field enhancement in the vicinity of the metal surface for the parameters listed above. In particular, in each figure the continuous line is the amplitude reflectivity, and the dashed line is the ratio of the absolute square of the magnetic fields at the metal surface and inside the prism as a function of the angle of incidence. Figure 4(a) corresponds to t = 70 nm and Fig. 4(b) to t = 10 nm with only the long-range mode shown in the latter figure. For t = 10 nm the field enhancement can be seen to be ~1 order of magnitude larger than that obtainable in the case of the thicker metal film, which corresponds to the Otto geometry. Our calculations with the Kretschmann geometry show the enhancement to be essentially the same as those obtained in the Otto geometry.

In summary, we have presented a comparison between the properties of the surface-plasma waves excited by three different prism-coupling geometries. The analysis shows that our geometry can give rise to a field enhancement that can be 1 order of magnitude larger than those obtainable by the two

other geometries. We plan to use our new geometry, where the light is guided along a very thin metal film, for nonlinear interactions such as second harmonic generation, four-wave mixing, and other power-dependent refractive-index phenomena.[6]

This work is supported in part by NSF grant ECS-8120348. One of us (RTD) wishes to thank Hyatt Gibbs for an invitation to spend a sabbatical at the Optical Sciences Center; he is on sabbatical leave from the University of Toledo.

References

1. A. Otto, Z. Phys. 216, 398 (1968).
2. E. Kretschmann, Z. Phys. 241, 313 (1971).
3. W. H. Weber and G. W. Ford, Opt. Lett. 6, 122 (1981).
4. D. Sarid, Phys. Rev. Lett. 47, 1927 (1981).
5. M. Born and E. Wolf, *Principles of Optics* (Pergamon, New York, 1964).
6. D. Sarid, R. T. Deck, and J. J. Fasano (submitted to J. Opt. Soc. Am.).

Optical field enhancement by long-range surface-plasma waves

Dror Sarid, Robert T. Deck, Alan E. Craig, Robert K. Hickernell, Ralph S. Jameson, and Joseph J. Fasano

Joseph Fasano is with U.S. Army, ARRADCOM, Dover, New Jersey 07801; the other authors are with University of Arizona, Optical Sciences Center, Tucson, Arizona 95721.

Received 21 May 1982.

Consider a TM polarized monochromatic wave that is incident on the base of a prism from which it is totally internally reflected. If a metallic substrate is placed in the vicinity of the prism so that the evanescent fields of the reflected light penetrate the metal, and the incident angle is appropriate, a surface-plasma wave can be excited along the metal gap. Otto[1] has analyzed this geometry and has shown both theoretically and experimentally that by measuring the reflectivity of a plane wave as a function of the angle of incidence one obtains both the speed and the range of the surface-plasma wave from the position of the minimum and the width of the Lorentzian absorption curve, respectively. In his geometry the metal thickness was much larger than the decay length of the surface-plasma field in the metal. Kretschmann[2] considered a different geometry in which a thin metal film is deposited on the bottom of the prism and a plane wave incident on the base of the prism excites a surface-plasma wave on the lower side of the metal film. The excitation in this case takes place via the optical fields that penetrate the metal. As with the Otto geometry, the excitation is possible because the speed of the surface-plasma wave is slower than the speed of the light in the prism.

Weber and Ford[3] have recently shown that the fields accompanying the surface-plasma wave are larger than those associated with total internal reflection in the absence of surface-plasma waves. In their theory they assume a general coupling mechanism that is 100% efficient and equate the optical power density injected by the coupler under steady state conditions to the power dissipated by the surface-plasma wave.

They show that the excitation of a surface-plasma wave at an optical frequency can give rise to an enhancement of the optical electric fields at a silver metal surface by a factor as large as 60. Their theory, however, is approximate because in calculating the enhanced fields they use the free surface-plasma fields instead of the true fields in the presence of the excitation medium (a prism or a grating, for example.)

In this Letter we wish to show theoretically that (1) it is possible to obtain an exact solution to the field enhancement for both the Otto and the Kretschmann geometries and (2) our new geometry[4] makes it possible to obtain field enhancements that are as much as an order of magnitude larger than those obtainable with the two other geometries.

The three prism-coupling geometries are shown in Fig. 1, where I and III correspond to the Otto and Kretschmann geometries, respectively, and II to our geometry. In each case

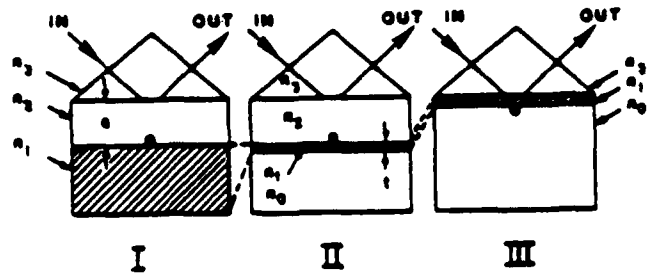

Fig. 1. Three prism-coupling geometries for exciting a surface-plasma wave: I, III, and II correspond to the Otto, Kretschmann, and our geometries, respectively.

t denotes the metal thickness, and the black dot in each diagram indicates the point where the optical fields are evaluated. In geometries I and II the evanescent fields created at the prism surface need to penetrate an intermediate medium separating the prism and the metal film. The exponential decay of the field amplitude in this medium is expressed by the factor $h = \exp(-KCS)$, where $K = 2\pi/\lambda$, λ is the optical wavelength in free space, S and n_2 are the thickness and refractive index of the gap, $C^2 = \beta^2 - n_2^2$, and $K\beta$ is the propagation constant of the surface-plasma wave which has only a real part for the plane wave approximation. In this work we assume a varying thickness S so that $h = 0.1$ for any given angle. The reason for this choice is that under these conditions the reflectivity obtains its minimum value for the appropriate angle for most of the cases we consider. It can be seen that geometry II merges into the Otto geometry for t sufficiently large and $h < 1$ and into the Kretschmann geometry for t sufficiently small and $h = 1$. For geometry II to be maximally effective, the refractive indices of the media bounding the metal film on either side need to be approximately the same.

Now in the general case of a stratified medium characterized by complex dielectric constants the reflectivity of a TM polarized monochromatic plane wave at the surface of the medium and the fields excited in each of the media can be computed by standard techniques.[5] For the plane wave assumption to be applicable to our geometry it is necessary that the range of the surface-plasma wave be appreciably smaller than the width of the incident optical beam. In the visible range of the spectrum, where the latter range is <1 mm, this requirement is easily satisfied, and the simple plane wave calculations yield accurate results for all three geometries.

To demonstrate the field enhancement obtainable with our geometry we choose parameters appropriate to the case of a silver metal film having a dielectric constant given by $-16 + i0.52$ at a wavelength of 632.8 nm, bounded by two dielectric media having a refractive index of 1.5. Our prism is assumed to be rutile with a refractive index of 2.875. Figure 2 shows the amplitude reflectivity at the base of the prism for three metal film thicknesses: $t = 2000$, 70, and 50 nm with $h = 0.1$. Note how the single Lorentzian absorption curve associated with the thick metal film splits into two Lorentzians as the film thickness decreases. The splitting is a direct result of the lifting of the degeneracy in the propagation constants of the

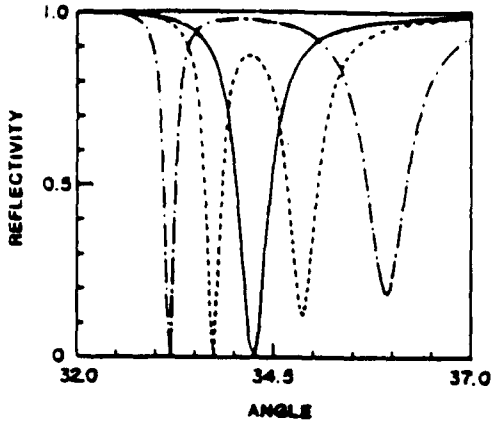

Fig. 2. Reflectivity as a function of the incident angle inside the prism for our geometry where $n_0 = n_2$. (—), (---), and (—·—) are for t = 2000, 70, and 50 nm, respectively. Note the splitting of the single Lorentzian into two Lorentzians as the metal film thickness decreases. The wide and the narrow Lorentzians correspond to the short-range and long-range surface-plasma waves, respectively.

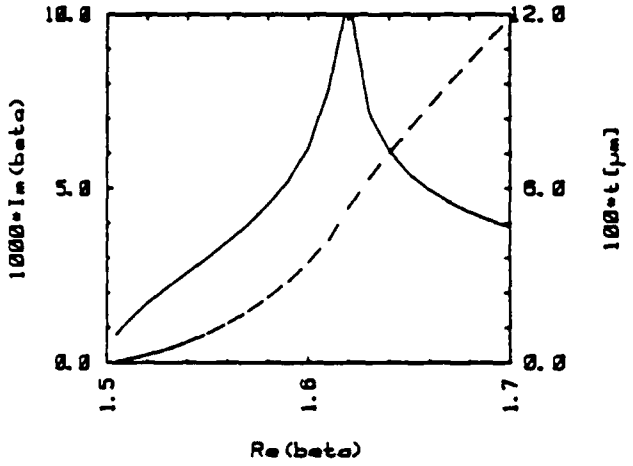

Fig. 3. Dispersion curves of the free surface-plasma waves: Im(β) (dashed line) and t (continuous line) as a function of Re(β). Note the divergence of t for Re(β) that corresponds to the thick metal case, and the two values of Re(β) and Im(β) for each t for the thinner metal case.

two independent surface-plasma waves propagating on each surface of the thick metal. Once the metal film thickness becomes small enough, the fields of these two surface-plasma waves inside the metal overlap, and the degeneracy is lifted. For such a thickness, one long-range and one short-range surface-plasma wave can be excited as a single eigenmode that satisfies all the boundary conditions simultaneously.[4] One observes that the Lorentzian width at half maximum for the short-range and for the long-range mode increases and decreases, respectively. The width consists of two contributions, one from the power dissipation in the metal film and one from the prism loading. This analysis differs from that of Weber and Ford, because it takes into account the important fact that any efficient means of excitation has in principle to interfere with the excited system which can no longer be considered to exist as a free one. In this respect our analysis is more accurate.

Figure 3 shows the dispersion curves of the free surface-plasma waves in the absence of the prism loading. The dashed and continuous curves show, respectively, the imaginary part of β and the metal thickness t as a function of the

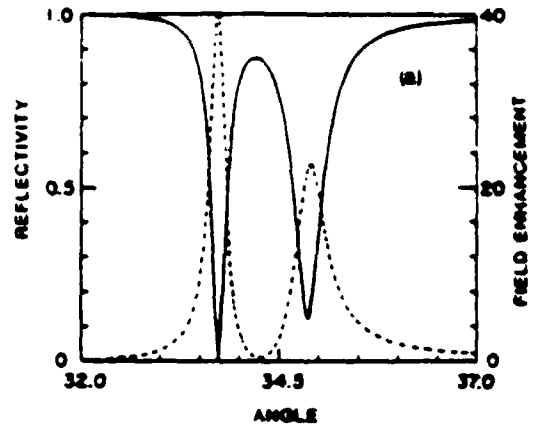

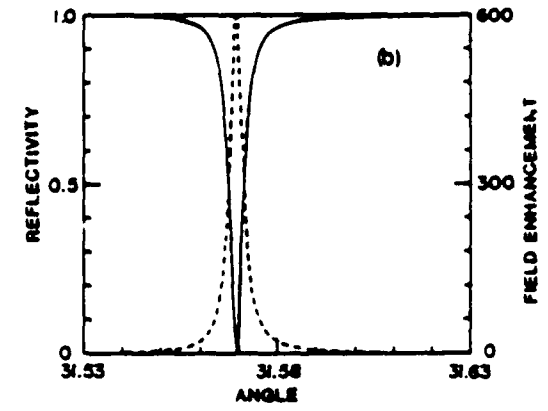

Fig. 4(a) Reflectivity (continuous line) as a function of the incident angle and the ratio of the absolute square of the magnetic fields at the metal surface and inside the prism (dashed line) for t = 70 nm. (b) Same as (a) but with t = 10 nm. Note the enhancement of the optical fields relative to the thick metal case.

real part of β. One observes the divergence of t for a value of β which corresponds to the degenerate case discussed before. For smaller values of t one obtains two values for both the real and imaginary parts of the propagation constant, each pair of real and imaginary values corresponding to either the short-range or the long-range mode. In the presence of the prism loading (with h = 0.1) the Lorentzian width shown in Fig. 2 is approximately a factor of 2 larger than the one computed from Im(β) in Fig. 3. The chosen value of h, therefore, has the effect of roughly equalizing the plasma-wave losses associated with reradiation and dissipation in the metal.

In Figs. 4(a) and (b) we show the field enhancement in the vicinity of the metal surface for the parameters listed above. In particular, in each figure the continuous line is the amplitude reflectivity, and the dashed line is the ratio of the absolute square of the magnetic fields at the metal surface and inside the prism as a function of the angle of incidence. Figure 4(a) corresponds to t = 70 nm and Fig. 4(b) to t = 10 nm with only the long-range mode shown in the latter figure. For t = 10 nm the field enhancement can be seen to be ~1 order of magnitude larger than that obtainable in the case of the thicker metal film, which corresponds to the Otto geometry. Our calculations with the Kretschmann geometry show the enhancement to be essentially the same as those obtained in the Otto geometry.

In summary, we have presented a comparison between the properties of the surface-plasma waves excited by three different prism-coupling geometries. The analysis shows that our geometry can give rise to a field enhancement that can be 1 order of magnitude larger than those obtainable by the two

interactions such as second harmonic generation, four-wave mixing, and other power-dependent refractive-index phenomena.[6]

This work is supported in part by NSF grant ECS-8120348. One of us (RTD) wishes to thank Hyatt Gibbs for an invitation to spend a sabbatical at the Optical Sciences Center; he is on sabbatical leave from the University of Toledo.

1. A. Otto, Z. Phys. 216, 398 (1968).
2. E. Kretschmann, Z. Phys. 241, 313 (1971).
3. W. H. Weber and G. W. Ford, Opt. Lett. 6, 122 (1981).
4. D. Sarid, Phys. Rev. Lett. 47, 1927 (1981).
5. M. Born and E. Wolf, *Principles of Optics* (Pergamon, New York, 1964).
6. D. Sarid, R. T. Deck, and J. J. Fasano (submitted to J. Opt. Soc. Am.).

Reprinted from Optics Letters, Vol. 8, page 380, July, 1983

Experimental observation of the long-range surface-plasmon polariton

Alan E. Craig, Grieg A. Olson, and Dror Sarid

Optical Sciences Center, University of Arizona, Tucson, Arizona 85721

Received April 4, 1983

The propagation and attenuation constants of long-range surface-plasmon polaritons propagating on thin metal films have been measured for several film thicknesses by using a hemispherical retroreflecting coupler. The results are in agreement with our theoretical dispersion curves, which predict that the attenuation constant of this mode can decrease by a factor of 63 relative to that obtained with a thick metal film.

It is well known by now that surface-plasmon polaritons that propagate on a thin metal film split into two branches, denoted as the short- and the long-range modes, when the thickness of the metal film on which they propagate decreases below a critical value of about 100 nm.[1,2] The main features of the long-range mode, which is the one of interest, are that, as the thickness of the metal film decreases, both its propagation and decay constants (the inverse of the range) decrease, while amplitudes of the electric and magnetic fields associated with this mode increase. As a result, nonlinear interactions involving the long-range mode, such as second-harmonic generation[3] and the intensity-dependent propagation constant,[4,5] will be greatly enhanced.

Previous measurements of the real and imaginary components of the propagation constant of surface-plasmon polaritons propagating on thin metal films (down to 50 nm) have indicated that both of these components decrease as the metal film thickness decreases.[6] In this Letter we present experimental results in which the reflectivity from very thin metal films (down to 10 nm) was measured as a function of the angle of incidence. These results, obtained by a computerized system that incorporates a hemispherical retroreflecting coupler together with an index-matching fluid, are in agreement with our previously published theoretical dispersion curves.

In fitting the reflectivity measurements with the theory, we use only the Fresnel equations with complex refractive indices and the dispersion equation of the free surface-plasmon polaritons.

Our system consists of three parts, the computer-controlled electronics, the optical-beam-shaping components, and the hemispherical retroreflecting coupler. We use a microcomputer to drive a step-motor-driven rotary table with a reproducible angular resolution of 1/240 deg.

Light from a He–Ne laser operating at a wavelength of 632.8 nm passes through a 1-kHz chopper, a spatial filter, a beam expander, a square aperture, and a beam-shaping lens. The beam is next incident upon a hemispherical coupler that was cut in half, metallized, and then glued back together, as shown in Fig. 1. The lens preceding the coupler ensures that the beam inside it is collimated. The beam is retroreflected by the hemispherical coupler, first from the metallized surface, then from the coupling surface, so that at any given angle of incidence the reflected beam is parallel to the incident one. These two beams are then separated by a pellicle beam splitter, and the reflected one is focused onto a photodetector.

The hemispherical coupler presses on a thin metal film deposited on top of a specially polished flat glass slide. An index-matching fluid fills the gap separating the coupler and the metal film, providing a symmetric refractive-index structure bounding the metal film. The glass slide is supported by three ball bearings, which are spring mounted on separate micrometers. The gap can therefore be adjusted in both magnitude and shape to conform to the optimal coupling specifications.

The microcomputer drives the stepping motor, which

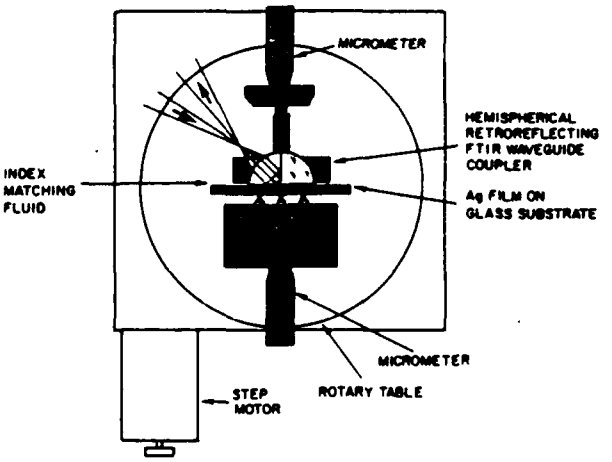

Fig. 1. The hemispherical retroreflecting coupler showing the three ball-bearing pressure points for shaping the gap that separates the coupler from the metal film. An index-matching fluid fills the gap and makes it possible to excite the long-range surface-plasmon polariton.

0146-9592/83/070380-03$1.00/0

in turn rotates the turntable, while the detector monitors the intensity of the reflected beam. The signal from the photodetector is fed into a lock-in amplifier, converted into a digital signal, and transferred to the microcomputer. A plotter then records the reflected beam intensity as a function of the beam angle of incidence on the base of the coupler.

In the vicinity of the resonance angle of the surface-plasmon polariton, the reflected beam decreases in intensity because of the dissipation of the optical power carried by the excited mode. The FWHM of the registered Lorentzian absorption, together with the angle of maximum absorption, is measured. The pressure on each of the ball bearings is adjusted several times, and for each adjustment the width and the location of the Lorentzian absorption are measured. From these results one obtains the natural width and location of the Lorentzian absorption that is due to the dissipation of the optical power by the surface-plasmon polariton. The real and imaginary components of the dielectric constant are determined by adjusting their value in the theoretical reflectance calculation so that the angular location and width of the resonance match those of the experimental curve for the 200-nm-thick metal film. Once the dielectric constant is known, it is used to plot the real and imaginary components of the propagation constant for the two branches. The dielectric constant that we measured for the thick film, and that we have used for the analysis of the thinner films, is $-18.9 + i0.581$, which is typical of Ag.

For thinner films, we monitor their nominal thickness during evaporation and then adjust the theoretical thickness to a value such that the theoretically plotted Lorentzian absorption has its minimum at the same angle as that of the experimental one. We than take the ratio of the widths of the experimental and the theoretical Lorentzian absorptions and multiply the theoretical imaginary component of the propagation constant by the same ratio to obtain the experimental value.

We tested four Ag films, which were vacuum deposited slowly enough to permit approximate thickness measurement. For films thinner than 30 nm, the thickness above which Ag agglomeration islands disappear, the substrate was electron bombarded during evaporation. The films had the nominal thicknesses of 2000, 50, 13, and 10 nm. Each film thickness was monitored to an accuracy of about 20% at evaporation. The refractive indices of the coupler, the oil, and the glass were 1.7788, 1.50173, and 1.50231, respectively.

The solid and dotted curves of Fig. 2 show the theoretical values of the real and the imaginary components, respectively, of the propagation constant of the two surface-plasmon polariton modes. One observes that, as the metal film thickness decreases, both the real and the imaginary components decrease for one mode and increase for the other one, which makes it possible to distinguish between the two experimentally. The agreement between the theoretical and the experimental imaginary components is only within a factor of 2 because of differences in the effective dielectric constants of the thick and thin films.

The trend toward lower losses (and concomitant

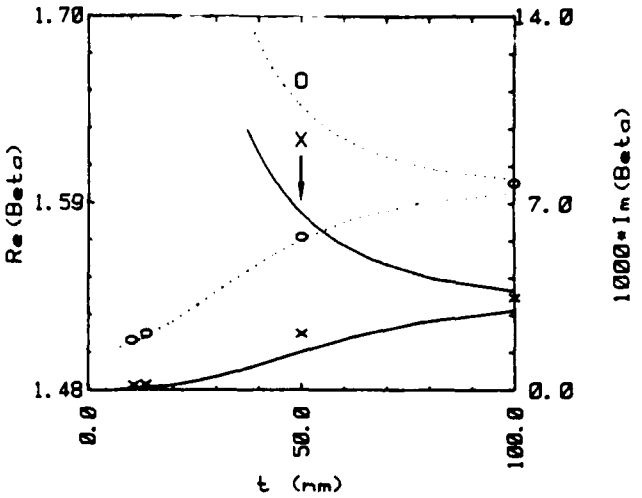

Fig. 2. The theoretical results of the real (dotted curve) and the imaginary (solid curve) components of the propagation constant as a function of the metal film thickness t. The upper and lower branches describe the short- and long-range surface-plasmon polaritons, respectively. The experimental values of the real component of the propagation constant are marked by open ovals. The imaginary component (×) agrees within a factor of 2 with the theoretical results.

longer propagation distances) for modes propagating on thinner metal films is clear. For the case of the 10-nm-thick silver film, the thinnest film for which measurements of the angular width of the resonance have been made, 0.055 deg at FWHM was recorded. A substantial portion of this angular width is due to angular divergence of the laser beam at the coupling interface, estimated to be 0.044 deg. The difference between these two angles is contributed by the surface-plasmon polariton, from which we find that its range is 0.25 mm. This value is 63 times larger than the corresponding value when a thick metal film is used.

We have also observed the short-range mode. It exhibits a Lorentzian absorption having a FWHM that broadens and shifts farther from the critical angle as the thickness of the film is progressively decreased.

The procedure used to compare the experimental results with the theory neglects the important contribution that the preparation method of the film, the creation of cermets, surface roughness, and aging have on the value of the dielectric constant. Nevertheless, the experimental results indicate clearly that the real and the imaginary components of the propagation constant follow the theoretical prediction and that films as thin as 10 nm can be readily measured. Since the resonances obtained for the thin films are narrow, accurate measurements of small imperfections can easily be identified.

In summary, we present experimental results of the propagation and decay constants of the long-range surface-plasmon polariton and show that they are in agreement with the theoretical dispersion curves. The measurements were carried out down to 10-nm thin metal films, for which the range is increased by a factor of 63 relative to that obtained with thick films.

In the process of writing this Letter we have learned of the independent measurement of the long-range surface-plasmon polariton by J. C. Quail *et al.* of the University of Toledo, who were kind enough to send us a preprint of their work. The authors would like to thank Steve Browning and Fred Van Milligen for the preparation of the films. This work is supported by National Science Foundation grant ECS-8120348, Defense Advanced Research Projects Agency grant N60530-83-C-0089, and by the U.S. Air Force Office of Scientific Research (AFSC) and the U.S. Army Research Office.

References

1. D. Sarid, Phys. Rev. Lett. **47**, 1927 (1981).
2. D. Sarid, R. T. Deck, A. E. Craig, R. K. Hickernell, R. S. Jameson, and J. J. Fasano, Appl. Optics **21**, 3993 (1982).
3. R. T. Deck and D. Sarid, J. Opt. Soc. Am. **72**, 1613 (1982).
4. D. Sarid, R. T. Deck, and J. J. Fasano, J. Opt. Soc. Am. **72**, 1345 (1982).
5. G. I. Stegeman, J. J. Burke, and D. G. Hall, Appl. Phys. Lett. **41**, 906 (1982).
6. G. J. Kovacs and G. D. Scott, Phys. Rev. B **16**, 1927 (1977).

Reprinted from Applied Optics, Vol. 22, page 3397, November 1, 1983

Coupling between finite electromagnetic beam and long-range surface-plasmon mode

Robert T. Deck, Dror Sarid, Grieg A. Olson, and J. M. Elson

In this paper, we consider a layered structure consisting of dielectric, metal, and dielectric media and compute the fields produced in the structure by a finite width beam of incident radiation which couples to a long-range surface-plasmon mode in the metallic layer. The analysis allows for complex dielectric constants in all media and focuses on optical radiation. Curves are presented which show the profiles of the reflected field intensity for different values of the propagation length of the mode relative to the width of the incident beam. We discuss the conditions in which the field reradiated from the long-range surface mode can interfere with the specularly reflected radiation so as to produce an interference zero in the reflected profile. In these conditions our analysis allows for a determination of the separate loss coefficients of the mode associated with energy reradiation and dissipation, respectively

I. Introduction

There is continued interest in application of electromagnetic energy propagation along boundary interfaces and in thin film waveguides. The modes of field propagation involved will be referred to here as boundary layer modes. The fields of such modes effectively propagate on or parallel to the interface surfaces of a layered structure consisting of media of different dielectric properties.[1] Because the fields of the modes do not couple directly to volume electromagnetic fields, the excitation and detection of the modes require certain techniques.

A general description of the modes in the case of lossless thin film dielectric waveguides has been given by Tien and Ulrich[2] and Ulrich.[3] The present paper presents a similar description in the case where the guiding film is metallic and the media which bound it are in general lossy. In this case the propagating boundary layer modes correspond to surface-plasmon modes on the metal film.

A large number of papers have discussed the excitation and detection of surface-plasmon modes on the surface of a thick metal film (e.g., Refs. 4 and 5). However, recent work[6] has pointed to a new type of surface-plasmon mode that can propagate on the surfaces of a thin metal film. This new mode referred to as a long-range surface-plasmon wave (LRSPW) has a range of propagation which can be more than an order of magnitude larger than ranges previously observed. Because this new mode has possible applications as a sensitive probe of surface roughness and the dielectric properties of materials, we feel that it is important to have an overall description of the fields associated with such modes and of the effects which their presence has on the reflectivity of ideal multilayered surfaces. We give here a description of both in the case where the modes are excited through a prism coupler. The reflectivity is calculated in the cases where the incident beam has both an infinite and a finite width. In the latter case, with the incident beam assumed to be a square wave, we describe the profile of the reflected beam in the presence of a long-range surface-plasmon mode.

The effects of boundary layer modes on the profiles of reflected beams have been described in previous papers (e.g., Refs. 3, 7, and 8) in which losses due to dissipation are for the most part neglected. A description of the reflected profile of a Gaussian incident beam in the case of surface-plasmon excitation in a thick metal film is given in Ref. 9. Because the propagation length of a surface plasmon wave on a thick metal film decreases rapidly as the frequency of the wave increases, observable effects are obtained in Ref. 9 only at frequencies in the IR. In the present paper where we focus on the excitation of a LRSPW on a thin metal film, observable effects can be obtained even at frequencies corresponding to visible radiation, and in our applications we consider such radiation exclusively.

Robert Deck is with University of Toledo, Department of Physics & Astronomy, Toledo, Ohio 43606; J. M. Elson is with U.S. Naval Weapons Center, Physics Division, Michelson Laboratory, China Lake, California 93555; the other authors are with University of Arizona, Optical Sciences Center, Tucson, Arizona 85721.

Received 2 June 1983.

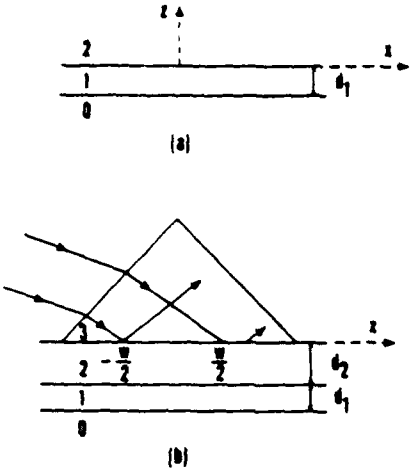

Fig. 1. (a) Geometry of boundaries between three media which define layered structure. (b) Geometry used to excite boundary layer mode on layered structure 2–1–0.

In Sec. II.A we present the general theory of excitation of a surface-plasmon mode by a plane electromagnetic wave, with the focus on the case where the coupling between the incident and plasmon fields can be considered weak. By use of a simple pole approximation in this case we develop simplified expressions for the reflection and transmission coefficients in the presence of the plasmon mode. Here the notation and style of Ref. 3 are followed, and for completeness certain details given there are repeated. In Sec. II.B the plane wave theory is made use of to develop expressions for the reflection and transmission coefficients in the case of plasmon excitation by a finite width electromagnetic wave. The results we obtain represent generalizations of the equations of Ref. 3 for the case of lossy media. In particular, we allow for complex dielectric constants in all media except the coupling prism. We make use of our results applied to the case of an incident square wave to describe a method of analysis by which it is possible to determine the separate loss coefficients of the mode associated with energy reradiation and dissipation.

In Sec. III the formulas developed in Sec. II are applied to a specific case of excitation of a long range surface-plasmon mode by a square wave He–Ne beam. Here we present curves showing the profiles of the reflected field intensity for various ranges of propagation of the mode relative to the width of the incident beam. Finally in the Appendix we give general formulas for two quantities associated with the surface modes considered.

II. General Theory

A. Mode Excitation by a Plane Wave

We are interested in the excitation of a boundary layer mode of the electromagnetic field within the layered structure defined by the 2–1 and 1–0 boundary surfaces shown in Fig. 1(a). By definition the fields of such a mode must decay exponentially away from both the 2–1 surface (in the $+z$ direction) and the 1–0 surface (in the $-z$ direction) so as to propagate effectively only parallel to the boundary interfaces. For such a mode to exist the component of the propagation vector parallel to the interfaces k must satisfy a so-called dispersion equation expressible in the form[2,3]

$$\psi_{10}(\beta) = 2k_{1z}d_1 - 2\phi_{12} - 2\phi_{10} = 2m\pi, \qquad m = 0,1,2, \ldots \quad (1)$$

Here use is made of the notation

$$k = \frac{\omega}{c}\beta,$$

$$k_{jz} = \frac{\omega}{c}\sqrt{\epsilon_j - \beta^2},$$

$$\phi_{jl} = \frac{i}{2}\ln r_{jl}, \qquad j,l = 0,1,2,3, \quad (2)$$

where r_{jl} is equal to the amplitude reflection coefficient for reflection of a plane wave of wave vector $\mathbf{k}_j = (k\hat{x} + k_{jz}\hat{z})$ at a boundary surface separating two media with dielectric constants ϵ_j and ϵ_l, respectively. In the case (of interest) of a TM polarized wave

$$r_{jl} = \exp(-2i\phi_{jl}) = \frac{\epsilon_l k_{jz} - \epsilon_j k_{lz}}{\epsilon_l k_{jz} + \epsilon_j k_{lz}} = -r_{lj}, \quad (3)$$

$$\phi_{jl} = \tan^{-1}\left(\frac{\epsilon_j k_{lz}}{i\epsilon_l k_{jz}}\right). \quad (4)$$

The dispersion equation (1) can be derived from the (unphysical) requirement that the total reflection coefficient for reflection from the 2–1–0 (or 0–1–2) interface be equal to infinity. In particular, with the total reflection coefficient for the 2–1–0 interface written as

$$r_{210} = \frac{r_{21} + r_{10}\exp(2ik_{1z}d_1)}{1 + r_{21}r_{10}\exp(2ik_{1z}d_1)}, \quad (5)$$

the condition for a boundary layer mode derives from the requirement that the denominator of r_{210} vanish, or equivalently, that a pole occur in the quantity $[1 - r_{12}r_{10}\exp(2ik_{1z}d_1)]^{-1}$.

It is convenient to introduce the notation

$$R_0(\beta) = r_{12}r_{10}\exp(2ik_{1z}d_1). \quad (6)$$

With β_m defined to be a value of β for which R_0 equals unity, the pole condition equivalent to Eq. (1) assumes the form

$$R_0(\beta_m) = \exp|2i(k_{1z}d_1 - \phi_{12} - \phi_{10})|_{\beta_m} = \exp|i\psi_{10}(\beta_m)| = 1. \quad (1')$$

Expressed as the condition on the reflection coefficient, $r_{210} = \infty$, the mode condition defines a boundary layer mode on the 2–1–0 interface as a mode which persists in the absence of an incident field in medium 2. On the other hand, since the dispersion relation (1) is found to have only solutions with $k_\parallel$ greater than $\sqrt{\epsilon_2}\,(\omega/c)$, the k-vector of the boundary layer mode must exceed the propagation vectors of bulk electromagnetic waves in medium 2, and the mode can, therefore, be excited only by an evanescent wave in that medium.

In a so-called Otto configuration[10] an evanescent wave with $k = (\omega/c)\sqrt{\epsilon_3}\sin\theta_i > (\omega/c)\sqrt{\epsilon_2}$ is excited in medium 2 by an electromagnetic wave which is totally internally reflected at a boundary surface 3–2 that is separated from the 2–1 surface by a gap of distance d_2

[as in Fig. 1(b)]. The total internal reflection condition requires $\epsilon_3 > \epsilon_2$. In order that the amplitude of the evanescent field be large enough at the 2–1 surface to excite an observable mode on the 2–1–0 interface, the amplitude factor

$$h \equiv \exp(ik_{2z}d_2) = \exp\left[-\left(k_1^2 - \epsilon_2\frac{\omega^2}{c^2}\right)^{1/2} d_2\right] \tag{7}$$

must be sufficiently larger than zero, which requires that d_2 be sufficiently small.

In the case of interest in which medium 1 is metallic, the dielectric constant ϵ_1 of medium 1 is a complex number with a negative real part, and the fields of a boundary layer mode on the 2–1–0 interface are evanescent within medium 1 as well as within media 2 and 0. In this case, for TM polarized radiation, there exist for the mode number $m = 1$ in Eq. (1) two complex solutions of the dispersion equation for β_m. If the thickness d_1 of the metallic medium is sufficiently large, these two solutions correspond to independent surface-plasmon modes on the separate surfaces 2–1 and 1–0. In particular, where

$$\exp(2ik_{1z}d_1) = \exp\left[-\frac{2\omega}{c}d_1\sqrt{\beta^2 - \epsilon_1}\right]$$

is approximately zero in Eq. (6) (for large d_1), the dispersion equation $R_0(\beta_m) = 1$ reduces to the separate equations

$$\frac{1}{r_{10}} = 0, \qquad \epsilon_0 k_{1z} = -\epsilon_1 k_{0z}, \tag{8a}$$

$$\frac{1}{r_{12}} = 0, \qquad \epsilon_1 k_{2z} = -\epsilon_2 k_{1z}, \tag{8b}$$

which correspond to dispersion relations for independent surface-plasmon modes on the interfaces 1–0 and 1–2, respectively. As the thickness d_1 of the metallic medium is reduced, however, the evanescent tails of separate modes on the two interfaces overlap, and the formerly independent modes interact to produce two distinct modes characterized by electric field distributions in the metal that are, respectively, symmetric and antisymmetric with respect to the transverse direction. Because the mode with the antisymmetric field distribution has a smaller fraction of its total field inside the metallic medium and, therefore, suffers less dissipation, it has a longer propagation range than does the other mode. It is this long-range mode which is of primary interest in the present paper. Since the range of the mode is determined by the imaginary part of the mode k-vector, the long-range mode corresponds to a small value of $\mathrm{Im}\beta$.

In the presence of the 3–2 boundary the reflection coefficients r_{210} and r_{012} at the upper and lower surfaces of the layered structure need to be replaced by the respective coefficients r_{3210} and r_{0123} with r_{ijlm} defined by the equation

$$r_{ijlm} \equiv \frac{r_{ij} + r_{jlm}\exp(2ik_{jz}d_j)}{1 + r_{ij}r_{jlm}\exp(2ik_{jz}d_j)}. \tag{9}$$

The condition on β required for a boundary layer mode on the 2–1–0 interface is then expressible as the condition $r_{0123} = \infty$, which amounts to the requirement that a pole occur in the quantity

$$u(\beta) \equiv [1 - r_{123}r_{10}\exp(2ik_{1z}d_1)]^{-1}. \tag{10}$$

Because r_{123} is equal to the expression

$$r_{123} = \frac{r_{12} + r_{23}\exp(2ik_{2z}d_2)}{1 + r_{12}r_{23}\exp(2ik_{2z}d_2)}, \tag{11}$$

provided $h^2 = \exp(2ik_{2z}d_2)$ is sufficiently small, $r_{123} \simeq r_{12} + 0(h^2)$, and the poles of the quantity $u(\beta)$ are shifted only slightly from the poles of the quantity $[1 - R_0(\beta)]^{-1} = [1 - r_{12}r_{10}\exp(2ik_{1z}d_1)]^{-1}$. It follows that the values of β corresponding to modes of the interface 2–1–0 in the presence of the 3–2 boundary are approximately the same as those of the free interface. The shifts in the positions of the poles in the presence of the additional boundary result from leakage of energy out of the modes in the form of radiation into medium 3. This leakage adds an additional damping term to the mode propagation vector which appears as an additional positive component of $\mathrm{Im}\beta_1$.

1. *Case of Weak Coupling*

Where the parameter h of Eq. (7) is large, so that there is a strong coupling between medium 3 (the prism) and medium 1 (the metal), the additional damping term in the mode fields resulting from radiation into medium 3 causes boundary layer modes on the 2–1–0 interface to be rapidly extinguished. In the cases of most physical interest, therefore, the parameter h is restricted between limits imposed by the dual requirements that h^2 be sufficiently greater than zero to allow for excitation of an interface mode and sufficiently less than one to prevent the rapid extinction of the mode. In practice here we restrict the values of h^2 to lie in the interval between 0.01 and 0.1. In this case the coupling between media 1 and 3 is referred to as weak.

To compute the reflectivity of the 3–2–1–0 layered structure in the conditions of excitation of a surface-plasmon mode on the 2–1–0 interface we need to evaluate the amplitude reflection coefficient r_{3210} for reflection of a plane wave field from the 3–2 boundary in the presence of the boundary layer mode. For this purpose it is useful to reexpress r_{3210} in terms of the pole function $u(\beta)$ of Eq. (10) in the form

$$r_{3210} = v(\beta)u(\beta), \tag{12}$$

where

$$v(\beta) \equiv \frac{r_{32} + r_{32}r_{21}r_{10}\exp(2ik_{1z}d_1) + h^2[r_{21} + r_{10}\exp(2ik_{1z}d_1)]}{(1 + h^2r_{12}r_{23})}. \tag{13}$$

Under the assumption of weak coupling with $h^2 \ll 1$, the quantity r_{123} in $u(\beta)$ can be expressed to first order in h^2 in the form

$$r_{123} = r_{12}(1 + 2ih^2r_{23}\sin 2\phi_{12}), \tag{14}$$

and $u(\beta)$ can be approximated by the expression

$$u(\beta) = [1 - R(\beta)]^{-1}, \tag{10'}$$

where

$$\left.\begin{aligned} R(\beta) &= r_{12}r_{10}\exp(2ik_{1z}d_1)(1 + 2ih^2 r_{23}\sin 2\phi_{12}) \\ &= R_0(\beta)\left[1 + \frac{\delta R(\beta)}{R_0(\beta)}\right] = \exp[i\psi_0(\beta) + i\delta\psi(\beta)] \\ \delta\psi(\beta) &= 2h^2 r_{23}\sin 2\phi_{12}. \end{aligned}\right\} \quad (15)$$

The poles of $u(\beta)$ occur at values of β denoted $\hat{\beta}_m$ for which $R(\beta) = 1$. Equivalently the positions $\hat{\beta}_m$ of the poles are defined by the equation

$$\psi_0(\hat{\beta}_m) + \delta\psi(\hat{\beta}_m) = 2m\pi, \qquad m = 0,1,2,\ldots, \quad (16)$$

with the value of $\hat{\beta}_m$ shifted from the values β_m corresponding to the modes of the free 2–1–0 interface by an amount of order h^2:

$$\hat{\beta}_m = \beta_m + \delta\beta_m. \quad (17)$$

By Taylor expansion of ψ_0 and $\delta\psi$ about $\hat{\beta}_m = \beta_m$ and use of Eq. (1), Eq. (16) can be reexpressed as an approximate equation for $\delta\beta_m$:

$$\psi_0(\beta_m) + \left.\frac{d\psi}{d\beta}\right|_{\beta_m}\delta\beta_m + \delta\psi(\beta_m) \simeq 2m\pi,$$

$$\delta\beta_m \simeq -\delta\psi(\beta_m)\Big/\left.\frac{d\psi}{d\beta}\right|_{\beta_m} = -\left.\frac{2h^2 r_{23}\sin 2\phi_{12}}{\left(\frac{d\psi}{d\beta}\right)\Big|_{\beta_m}}\right|_{\beta_m}. \quad (18)$$

The imaginary part of $\delta\beta_m$ determines the additional damping of the mth boundary layer mode caused by the presence of the 3–2 boundary. A general expression is given in the Appendix for the quantity

$$\left.\frac{d\psi}{d\beta}\right|_{\beta_m}.$$

For a value of β in the vicinity of the value $\hat{\beta}_m$ the function $u(\beta)$ has the form of a simple pole term with a coefficient determined by its Taylor expansion about $\hat{\beta}_m$. The result can be expressed in the approximate form

$$u(\beta) \simeq \frac{i}{\left.\frac{d\psi}{d\beta}\right|_{\beta_m}(\beta - \hat{\beta}_m)}. \quad (19)$$

To the same approximation the factor $v(\beta)$ of Eq. (13) can be written for β in the vicinity of $\hat{\beta}_m$ as

$$v(\beta) \simeq -i\left.\frac{d\psi}{d\beta}\right|_{\beta_m} r_{32}(\beta)\left[\beta - \beta_m - \frac{\delta\beta_m}{r_{32}^2(\beta_m)}\right]. \quad (20)$$

and the reflection coefficient r_{3210} can be reduced to the form

$$r_{3210}(\beta) \simeq r_{32}(\beta_m)\frac{\left[\beta - \beta_m - \frac{\delta\beta_m}{r_{32}^2(\beta_m)}\right]}{(\beta - \hat{\beta}_m)}, \quad (21)$$

where the slowly varying quantity $r_{32}(\beta)$ in (20) and (21) is approximated by its value at $\beta = \beta_m$.

Equation (21) represents a valid approximation to r_{3210} for a range of values of β centered on $\hat{\beta}_m$ and extending on either side of this value about half of the distance to the next pole of $u(\beta)$. Since the interval $\Delta\beta_m$ between the poles of $u(\beta)$ (in the vicinity of $\beta = \beta_m$) can be computed from the equation

$$\Delta\psi(\beta_m) = \left.\frac{d\psi}{d\beta}\right|_{\beta_m}\Delta\beta_m = 2\pi, \quad (22)$$

it results that Eq. (21) is valid for a range of β values given approximately by

$$\Delta\beta_m = 2\pi\Big/\left.\frac{d\psi}{d\beta}\right|_{\beta_m}. \quad (22)'$$

By use of Eq. (17), Eq. (21) can be reexpressed in an alternate form as the equation

$$r_{3210}(\beta) = r_{32}(\beta_m)\left\{1 + \frac{\delta\beta_m\left[1 - \frac{1}{r_{32}^2(\beta_m)}\right]}{\beta - \mathrm{Re}(\beta_m + \delta\beta_m) + i\,\mathrm{Im}(\beta_m + \delta\beta_m)}\right\}. \quad (23)$$

For β in the vicinity of $\hat{\beta}_m$ the absolute square of the bracket on the right-hand side of this equation exhibits a Lorentzian dip as a function of β centered at $\beta = \mathrm{Re}(\beta_m + \delta\beta_m)$, with a width Γ given by $\mathrm{Im}(\beta_m + \delta\beta_m) = \mathrm{Im}\hat{\beta}_m$. Therefore, since β is determined by the angle of incidence θ_i on the 3–2 boundary by the relation

$$\beta = \frac{c}{\omega}k_1 = \frac{c}{\omega}k\sin\theta_i = \sqrt{\epsilon_3}\sin\theta_i, \quad (24)$$

the reflectivity R defined by $|r_{3210}(\beta)|^2$ exhibits a Lorentzian shape as a function of $\sin\theta_i$ with its center at $(\theta_i)_0$ given by $\sqrt{\epsilon_3}\sin(\theta_i)_0 = \mathrm{Re}(\beta_m + \delta\beta_m) = \mathrm{Re}\hat{\beta}_m$. Where the metallic medium 1 is sufficiently thin in this case, the two solutions of the mode dispersion relation for $m = 1$, corresponding to the distinct surface-plasmon modes on the metal film, appear in the reflectivity as separate Lorentzians whose angular positions and widths, respectively, determine the real and imaginary parts of the $\hat{\beta}_m$ values for the separate modes. The Lorentzian corresponding to the long-range surface-plasmon mode is distinguished by its narrower width from that corresponding to the shorter range mode.

By way of the approximations used to obtain the above result for r_{3210} it is possible to derive a reduced expression for the amplitude transmission coefficient t_{321} connecting the amplitude of an incident field in medium 3 and the amplitude of the resulting field in medium 1. In general the resulting field in medium 1 is the resultant of the field transmitted through the 2–1 boundary and the fields multiply reflected at the 1–0 and 1–2–3 interfaces. Since the effect of the latter reflected fields on the amplitude of the field in medium 1 is expressible in terms of the z-dependent factor

$$a(\beta,z) = |\exp(ik_{1z}z) + r_{10}\exp[-ik_{1z}z + 2ik_{1z}(d_1 + d_2)]|, \quad (25)$$

it follows that the ratio of the amplitudes of the fields in media 1 and 3 is given by the product

$$a(\beta,z)t_{321}(\beta),$$

where, for the geometry of Fig. 1, t_{321} can be written in terms of $u(\beta)$ in the form

$$t_{321}(\beta) = \frac{(1 + r_{32})(1 + r_{21})}{1 + r_{32}r_{21}\exp(2ik_{2z}d_2)}u(\beta)\exp[i(k_{2z} - k_{1z})d_2]. \quad (26)$$

Use of Eqs. (19) and (25) and mode condition (1)′ subsequently reduces the product $a(\beta,z)t_{321}(\beta)$ to the approximate result

$$a(\beta,z)t_{321}(\beta) \simeq -i\frac{\bar{t}_m(\beta_m,z)}{(\beta-\beta_m)}, \tag{27}$$

with $\bar{t}_m$ given by

$$\bar{t}_m(\beta_m,z) = -2ih\frac{(1+r_{32})}{\left.\frac{d\psi}{d\beta}\right|_{\beta_m}}\sin\phi_{12} \times \{\exp[ik_{1z}(z-d_2)-i\phi_{12}| + \exp[-ik_{1z}(z-d_2)+i\phi_{12}]\}|_{\beta_m}. \tag{28}$$

B. Mode Excitation by Finite Width Beam

The (plane wave) results of the previous section can be applied to the interaction of a finite width electromagnetic beam with the multilayered structure of Fig. 1(b) by decomposition of the incident, reflected, and refracted beams into plane wave components. Consider in particular a beam with finite width in the x-z plane incident on the boundary surface 3–2 at $z = 0$. For simplicity we can assume that the beam has an unlimited width in the y direction and consists of radiation of a single frequency ω. Since the conditions for excitation of a surface-plasmon mode require TM radiation, we take the beam to be TM polarized with its magnetic field vector perpendicular to the x-z plane. Because the electric field components of the beam are related to the magnetic field component by Maxwell's equations, it is sufficient to consider only the latter field component. At $z = 0$ this component has the general form

$$B_3(x,t) = B_{3y}(x,z,t)|_{z=0} \equiv B_3(x)\exp(-i\omega t), \tag{29}$$
$$B_3(x) = F(x)\exp(ik_x^0 x),$$

where k_x^0 represents the average value of the x components of the propagation vectors in the incident beam and $F(x)$ is a lateral form factor determined by the transverse shape and width of the beam.

By Fourier decomposition the field $B_3(x)$ can be expressed as an integral over its plane wave components associated with distinct values of $\beta = (c/\omega)k_\parallel$ in the standard form

$$B_3(x) = \int_{-\infty}^{\infty} d\beta b_3(\beta)\exp\left(i\frac{\omega}{c}\beta x\right) \tag{30}$$

with

$$b_3(\beta) = \frac{\omega/c}{2\pi}\int_{-\infty}^{\infty} dx F(x)\exp\left[i\left(k_x^0 - \frac{\omega}{c}\beta\right)x\right]. \tag{31}$$

Each plane wave component in $B_3(x)$ contributes a plane wave term to the reflected field $B_3'(x)$ in medium 3 and to the transmitted field $B_1(x,z)$ in medium 1 determined by the respective plane wave reflection and transmission coefficients $r_{3210}(\beta)$ and $a(\beta,z)t_{321}(\beta)$, and the total fields $B_3'(x)$ and $B_1(x,z)$ can, therefore, be expressed in the forms

$$B_3'(x) = \int_{-\infty}^{\infty} d\beta r_{3210}(\beta)b_3(\beta)\exp\left(i\frac{\omega}{c}\beta x\right), \tag{32}$$

$$B_1(x,y) = \int_{-\infty}^{\infty} d\beta a(\beta,z)t_{321}(\beta)b_3(\beta)\exp\left(i\frac{\omega}{c}\beta x\right). \tag{33}$$

By introduction of Fourier transforms of $r_{3210}(\beta)$ and $a(\beta,z)t_{321}(\beta)$ and use of the convolution theorem, Eqs. (32) and (33) can be rewritten as the equations

$$B_3'(x) = \frac{\omega/c}{2\pi}\int_{-\infty}^{\infty} dx' R_{3210}(x-x')B_3(x'), \tag{34a}$$

$$B_1(x,z) = \frac{\omega/c}{2\pi}\int_{-\infty}^{\infty} dx' T_{321}(x-x',z)B_3(x'), \tag{35a}$$

where

$$R_{3210}(x) \equiv \int_{-\infty}^{\infty} d\beta r_{3210}(\beta)\exp\left(i\frac{\omega}{c}\beta x\right). \tag{34b}$$

$$T_{321}(x,y) \equiv \int_{-\infty}^{\infty} d\beta a(\beta,z)t_{321}(\beta)\exp\left(i\frac{\omega}{c}\beta x\right). \tag{35b}$$

Under the assumption that the incident field $B_3(x)$ is well collimated, the range $\Delta\beta$ of β values over which $b_3(\beta)$ is nonzero is determined strictly by the spatial width w of the incident beam through the relation $(\omega/c)\Delta\beta w \simeq 2\pi$ or

$$\Delta\beta \simeq 2\pi/(\omega/c)w. \tag{36}$$

Provided $\Delta\beta$ is less than or equal to the approximate spacing (in β space) between the surface modes of the 2–1–0 boundary interface, as defined by Eq. (22)′, the function $b_3(\beta)$ will overlap strongly with only one of the resonance poles of the functions $r_{3210}(\beta)$ and $t_{321}(\beta)$ in the integrals (32) and (33), and in general the incident beam will excite only one of the modes of the interface. For $(c/\omega)k^0$ in the vicinity of β_m the requirement $\Delta\beta \leq \Delta\beta_m$ imposes on w only the condition

$$\frac{\omega}{c}w \geq \left.\frac{d\psi}{d\beta}\right|_{\beta_m}, \tag{37}$$

which is easily satisfied in the cases considered below.

Given that relation (37) is satisfied, the functions r_{3210} and at_{321} in the integrands of Eqs. (32) and (33) [and, therefore, (34b) and (35b)] can be well approximated by their single-pole forms defined by Eqs. (21) and (27), and (with $\mathrm{Im}\beta_m$) constrained by causality to be positive) the Fourier transforms R_{3210} and T_{321} can be reduced to the expressions

$$R_{3210}(x-x') = r_{32}(\beta_m)\left\{\frac{2\pi}{\omega/c}\delta(x-x') + i\delta\beta_m\left[1-\frac{1}{r_{32}^2(\beta_m)}\right]\zeta_m(x-x')\right\}, \tag{38}$$

$$T_{321}(x-x',z) = \bar{t}_m(\beta_m,z)\zeta_m(x-x'), \tag{39}$$

where

$$\zeta_m(x-x') \equiv \begin{cases} 2\pi\exp\left[i\frac{\omega}{c}\beta_m(x-x')\right], & x' \leq x, \\ 0, & x' > x. \end{cases} \tag{40}$$

In this case by use of Eqs. (34a) and (35a) the fields $B_3'(x)$ and $B_1(x,a)$ assume the forms

$$B_3'(x) = r_{32}(\beta_m)B_3(x) + 2\frac{\omega}{c}\delta\beta_m\sin 2\phi_{32}(\beta_m) \times \int_{-\infty}^{x} dx' B_3(x')\exp\left[i\frac{\omega}{c}\beta_m(x-x')\right] \tag{41}$$

$$B_1(x,z) = \frac{\omega}{c}\bar{t}_m(\beta_m,z)\int_{-\infty}^{x} dx' B_3(x')\exp\left[i\frac{\omega}{c}\beta_m(x-x')\right], \tag{42}$$

with

$$\sin 2\phi_{32}(\beta_m) = \frac{i}{2}\left[r_{32}(\beta_m) - \frac{1}{r_{32}(\beta_m)}\right].$$

The first term on the right in Eq. (41) represents the field produced by the direct reflection of the incident field B_3 at the 3–2 boundary, which would occur in the absence of the additional 2–1 and 1–0 boundaries, while the second term on the right accounts for the influence of the latter boundaries and can be identified as the field which is reradiated back out of the boundary layer mode.

The rapidly varying x dependences of the fields B_3, B_3', and B_1 derive from rapidly varying x-dependent phases, which are approximately determined by the central k-vector $\mathbf{k}_3^0$ of the incident field B_3. As a consequence, by extracting the rapidly varying phase factor $\exp(i\mathbf{k}_3^0 x)$ from the fields, a set of more slowly varying field functions can be obtained which have x dependences that more closely characterize the more important spatial variations of the fields. In what follows we denote the more slowly varying field functions by a tilde symbol and connect them to the fields of Eqs. (41) and (42) by the relations

$$\tilde{B}_3(x) = B_3(x)\exp(-i\mathbf{k}_3^0 x), \qquad \tilde{B}_3'(x) = B_3'(x)\exp(-i\mathbf{k}_3^0 x),$$
$$\tilde{B}_1(x,z) = B_1(x,z)\exp(-i\mathbf{k}_3^0 x). \tag{43}$$

Following Ref. 3 the integral Eqs. (41) and (42) can be replaced by coupled (differential) equations for the fields B_3' and B_1 in terms of the incident field B_3. In particular, by differentiation of Eq. (42) with respect to x and use of Eq. (42) in (41), we derive two coupled equations, which in terms of the slowly varying field functions $\tilde{B}_1(x,z)$ and $\tilde{B}_3'(x)$ assume the forms

$$\frac{d\tilde{B}_1}{dx} = i\frac{\omega}{c}(\beta_m - k_3^0)\tilde{B}_1 + \frac{\omega}{c}\bar{t}_m\tilde{B}_3, \tag{44}$$

$$\tilde{B}_3' = r_{32}\tilde{B}_3 + 2\frac{\delta\beta_m}{\bar{t}_m}\sin(2\phi_{32})\tilde{B}_1, \tag{45}$$

where $k_3^0 \equiv (c/\omega)\mathbf{k}_3^0$ and r_{32}, $\bar{t}_m$, and ϕ_{32} are evaluated at $\beta = \beta_m$.

It is convenient to introduce the notation

$$\beta_m \equiv \beta' + i\beta''$$
$$\alpha \equiv -i\frac{\omega}{c}(\beta_m - k_3^0) = \frac{\omega}{c}(\beta'' + \mathrm{Im}\delta\beta_m) + i\frac{\omega}{c}(\mathrm{Re}\beta_m - k_3^0), \tag{46}$$
$$\alpha_1 \equiv -\frac{\omega}{c}\delta\beta_m \sin 2\phi_{32},$$

where $(\omega/c)\beta'$ and $(\omega/c)\beta''$ represent, respectively, the real and imaginary parts of the propagation vector of the mth boundary layer mode in the absence of the 3–2 boundary (with the mode label m suppressed). In this notation Eqs. (44) and (45) assume the simplified forms

$$\frac{d\tilde{B}_1}{dx} = -\alpha\tilde{B}_1 + \frac{\omega}{c}\bar{t}_m\tilde{B}_3, \tag{44}'$$

$$\tilde{B}_3' = r_{32}\tilde{B}_3 - \frac{2\alpha_1}{(\omega/c)\bar{t}_m}\tilde{B}_1. \tag{45}'$$

In regions of x beyond the point x_0 where the incident field at the 3–2 surface terminates, $B_3(x) \equiv 0$, and the solutions $\tilde{B}_3'$ and $\tilde{B}_1$ of Eqs. (44)′ and (45)′ have x dependences expressed by the simple exponential $\exp[-\alpha(x - x_0)]$. The latter expresses the exponential decay of the boundary layer mode whose radiation accounts for the total field B_3 at values of $x > x_0$. The decay of the boundary layer mode reflects energy losses from the mode resulting from both energy radiation into medium 3 and energy dissipation in medium 1. The separate losses contribute the separate positive terms $(\omega/c)\,\mathrm{Im}\delta\beta_m$ and $(\omega/c)\,\mathrm{Im}\beta_m$ to $(\omega/c)\,\mathrm{Im}\beta_m$, which appears as the positive real part of α. In the long-range surface-plasmon mode emphasized in the present paper, the energy losses due to dissipation are minimized.

1. *Case of Square Wave Input*

In the present section we evaluate the fields B_3' and B_1 in the example case of an incident beam in medium 3 which has a profile as a function of x that closely approximates a square wave. In this case the lateral form factor $F(x)$ in Eq. (29) can be represented as the discontinuous function

$$F(x) = \begin{cases} 0, & x < -\dfrac{w}{2}, \\ A, & -\dfrac{w}{2} \le x \le \dfrac{w}{2}, \\ 0, & x > \dfrac{w}{2}. \end{cases} \tag{47}$$

where w defines the length of intersection of the beam along the x axis [as shown in Fig. 1(b)]. Substitution of (29) and (47) into Eqs. (41) and (42) and evaluation of the required integrals lead to reflected and mode fields $\tilde{B}_3'$ and $\tilde{B}_1$ of the forms

$$\tilde{B}_3'(x) = r_{32}\tilde{B}_3(x) - \frac{2\alpha_1}{\alpha}A\,\|, \tag{48}$$

$$\tilde{B}_1(x) = \frac{(\omega/c)\bar{t}_m}{\alpha}A\,\|, \tag{49}$$

with

$$\|\equiv\begin{cases} 0, & x < -\dfrac{w}{2}, \\ \left\{1 - \exp\left[-\alpha\left(x + \dfrac{w}{2}\right)\right]\right\}, & -\dfrac{w}{2} \le x \le \dfrac{w}{2}, \\ -2i\exp(-\alpha x)\sin\left(i\alpha\dfrac{w}{2}\right), & x > \dfrac{w}{2}. \end{cases} \tag{50}$$

where α and α_1 are defined in Eqs. (46).

It follows from Eqs. (49) and (46) that the magnitude of the field in medium 1 is maximized for a given boundary layer mode m where the incident beam is tuned so that the central value of k_3^0, k^0 is equal to $(\omega/c)\,\mathrm{Re}\beta_m$. In this phase-matching condition (as pointed out in Ref. 3), the oscillating phase factor in the integrand of Eqs. (42) and (41) is nearly stationary, and the

coupling between the input field and the interface mode is optimized.

For a tuned input, the ratio $(2\alpha_1)/\alpha$ is predominantly real and positive, which means that for values of x between $-w/2$ and $w/2$ the two terms in Eq. (48) are of opposite sign. The resulting cancellation between the two terms, in certain conditions can produce an interference zero in the reflected field in the region of x where the incident beam intersects the 3–2 boundary. In these conditions, measurement of the position of the zero along with analysis of the profile of the reflected beam provides information about the excited interface mode, which cannot be extracted from measurements of the total reflectivity. In particular by measurement of both the position of the zero in the reflected profile and the rate of exponential decay of the tail of the profile (in the region $x > w/2$), the independent loss terms in the mode propagation constant associated with energy reradiation and dissipation can be determined separately. (In contrast a measurement of the width of the Lorentzian dip in the reflectivity as a function of θ_i provides only a determination of the total loss term $\mathrm{Re}\alpha$.)

Details of the analysis required to determine the separate loss constants $\mathrm{Im}\delta\beta_m$ and $\mathrm{Im}\beta_m$ are based on Eq. (48), which, for x in the interval $-w/2 \le x \le w/2$, gives the result[11]

$$\frac{\tilde{B}_3(x)}{\tilde{B}_3(0)} = r_{32} - \frac{2\alpha_1}{\alpha}\left\{1 - \exp\left[-\alpha\left(x + \frac{w}{2}\right)\right]\right\}. \tag{51}$$

For the right-hand side of Eq. (51) to vanish at a value of $x = x_1$ in the given interval, it is necessary that

$$\frac{2\alpha_1}{\alpha} n(x_1) = r_{32}, \tag{52}$$

where

$$n(x) \equiv \left\{1 - \exp\left[-\alpha\left(x + \frac{w}{c}\right)\right]\right\}.$$

With the beam tuned to a resonance zero in the reflectivity, the quantity α is purely real and equal to $(\omega/c)\,\mathrm{Im}\beta_m$, which value can be determined by measurement of either the width of the Lorentzian dip in the reflectivity or the decay rate of the exponential tail in the reflected profile (for $x > x_0 = w/2$). Using Eqs. (46), the real and imaginary parts of Eq. (52) give the two equations

$$\frac{\omega}{c}\mathrm{Im}\delta\beta_m = -\frac{\alpha}{2n(x_1)}\mathrm{Im}\left[\frac{r_{32}(\beta_m)}{\sin 2\phi_{32}(\beta_m)}\right], \tag{53a}$$

$$\frac{\omega}{c}\mathrm{Re}\delta\beta_m = -\frac{\alpha}{2n(x_1)}\mathrm{Re}\left[\frac{r_{32}(\beta_m)}{\sin 2\phi_{32}(\beta_m)}\right], \tag{53b}$$

where $n(x_1)$ can be computed from the measured value of x_1. The remaining factor on the right-hand side of Eqs. (53) can be rewritten in the form

$$\frac{1}{2}\left[\frac{r_{32}(\beta_m)}{\sin 2\phi_{32}(\beta_m)}\right] = -i[1 - 1/r_{32}^2(\beta_m)]^{-1}, \tag{54}$$

with $r_{32}(\beta_m)$ defined by the explicit formula

$$r_{32}(\beta_m) = \frac{\epsilon_2\sqrt{\epsilon_3 - \beta_m^2} - \epsilon_3\sqrt{\epsilon_2 - \beta_m^2}}{\epsilon_2\sqrt{\epsilon_3 - \beta_m^2} + \epsilon_3\sqrt{\epsilon_2 - \beta_m^2}}. \tag{55}$$

Since ϵ_2 and ϵ_3 are presumed known, an evaluation of Eq. (55) requires only the values of the real and imaginary parts of β_m. But the pole approximation underlying the present calculation assumes the slowly varying character of r_{32}, on the basis of which $r_{32}(\beta_m)$ must be approximately equal to $r_{32}(\beta_m)$. Therefore, to the accuracy of the present calculation, β_m can be replaced on the right-hand side of Eqs. (53) and (54) by β_m, the imaginary and real parts of which are determined by the measured value of α and the tuning angle of the mode, respectively:

$$\beta_m = \mathrm{Re}\beta_m + i\,\mathrm{Im}\beta_m = \sqrt{\epsilon_3}\sin\theta_i + i\frac{c}{\omega}\alpha. \tag{56}$$

Numerical evaluation of Eqs. (53) then allows evaluation of the loss constant $\mathrm{Im}\delta\beta_m$ and pole-shift $\mathrm{Re}\delta\beta_m$ associated with the mode radiation.

III. Numerical Results and Analysis

In Figs. 2 and 3 we plot the normalized reflected power P_r/P_i vs distance x along the 3-2 boundary for the case of a square wave He-Ne beam incident from a prism onto a dielectric-silver-dielectric interface with the central wave vector of the beam tuned to the long-range surface plasmon mode. The plotted curves are derived from the formula

$$\frac{P_r}{P_i} = \frac{|\tilde{B}_3(x)|^2}{|\tilde{B}_3(0)|^2}. \tag{57}$$

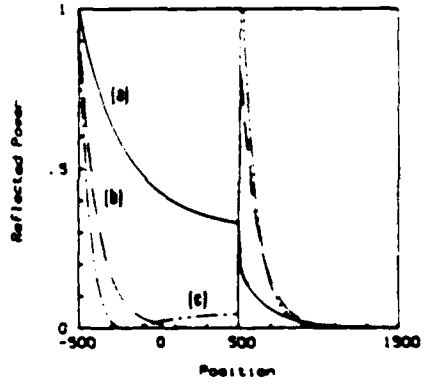

Fig. 2. Ratio of reflected power to incident peak power plotted as function of transverse distance along interface measured in microns. Position zero marks center of incident beam which extends from −500 to +500 μm. Parameters are as listed in text: (a) $d_2 = 1.25$ μm, $L/W = 0.35$; (b) $d_2 = 1$ μm, $L/W = 0.23$; (c) $d_2 = 0.9$ μm, $L/W = 0.174$.

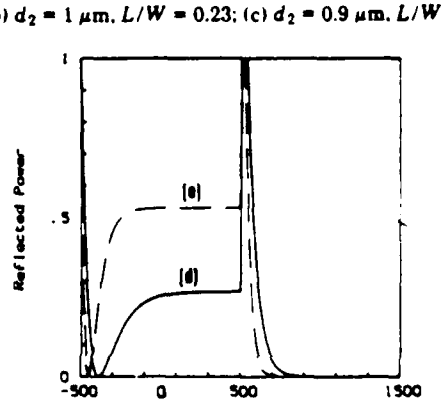

Fig. 3. Same as Fig. 2. (d) $d_2 = 0.75$ μm, $L/W = 0.106$; (e) $d_2 = 0.6$ μm, $L/W = 0.059$.

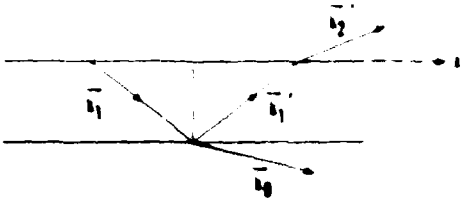

Fig. 4. Propagation vectors associated with boundary layer mode on layered structure 2-1-0.

with the ratio $\bar{B}_3(x)/\bar{B}_3(0)$ computed from Eqs. (48) and (50) and the vacuum wavelength λ and dielectric constants taken to be $\lambda = 6328$ Å, $\epsilon_0 = \epsilon_2 = (1.5)^2$, $\epsilon_1 = (1.72)^2$, $\epsilon_1 = \epsilon_{Ag} = -15.996 + 0.5256$. For the chosen parameters and an assumed metal film thickness d_1 of 200 Å the required angle of incidence θ_i is ~62°.

The distinct curves in Figs. 2 and 3 correspond to different values of the cover layer thickness d_2 with the beamwidth w fixed at 1 mm. The curves graph the distorted power profiles produced by the surface-plasmon mode, in the absence of which the reflected power profile must closely match the square profile of the incident beam. The distorted profiles result from a (partial) absorption of the energy of the incident beam into the mode and the subsequent reradiation of this energy back into the incident medium. Beyond the edge of the region illuminated by the incident beam (for $x > x_0 = w/2$), where the reflected power P_r derives strictly from the reradiated plasmon field, P_r decreases exponentially with a decay constant α given by $(\omega/c)\,\mathrm{Im}\beta_m$. On the other hand, for values of x within the illuminated region of the surface (for $-w/2 \le x \le w/2$), where the reflected power results from both the reradiatied field and the directly reflected incident field, destructive interference between these two fields results in a distorted square profile, details of which are determined for given dielectric parameters by the propagation length of the surface-plasmon mode in relation to the width of the incident beam. The shift of the centroid of the reflected profiles in Fig. 3 relative to that of the incident profile corresponds to the so-called Goos Hanchen shift.[8,12]

The propagation length L of the surface-plasmon mode, defined here as

$$L = \frac{1}{\omega/c\ \mathrm{Im}\beta_m} = \left[\frac{\omega}{c}(\beta'' + \mathrm{Im}\delta\beta_m)\right]^{-1}, \tag{58}$$

is determined by the (fixed) metal film thickness d_1, which determines the loss coefficient due to dissipation β'' and by the (varied) cover thickness d_2, which determines the loss coefficient due to reradiation $\mathrm{Im}\delta\beta$. Where the propagation length of the mode is short compared with the width of the beam, the plasmon field excited by the leading edge of the beam is reradiated strictly into the region illuminated by the beam. In this case the destructive interference between the reradiated field and the directly reflected field can produce a zero in the reflected profile in the region illuminated by the beam. To obtain a profile with a well-defined zero such as shown in curves (d) and (e) of Fig. 3 the ratio of the propagation length L to the beamwidth w needs to be restricted between definite limits of less than one. In the particular case shown in Figs. 2 and 3 the ratio L/w needs to be restricted between the limits 1.15 and 1.20. For larger values of L/w the intensity of the reradiated plasmon field is too weak in the region illuminated by the beam to produce an interference zero in that region, while for smaller values of L/w the interference zero can occur too close to the leading edge of the reflected beam to be observable. In practice, for a given input beamwidth, given that the plasmon losses in the metal are sufficiently small, an interference zero in the reflected profile can be obtained by adjustment of the cover thickness. In this case analysis of the profile described in Sec. II allows for determination of the separate loss coefficients β'' and $\mathrm{Im}\delta\beta$.

Appendix

In this Appendix we give an expression for the quantity $(d\psi)/(d\beta)$ in Eq. (18) and present a general formula for the power per unit length P carried by an interface mode. The result for P is valid for complex dielectric constants in media 2, 1, and 0 and represents a generalization of the formula given by Marcuse in Ref. 1.

We consider the case of mode excitation by TM polarized radiation with longitudinal k-vector $\mathbf{k}_z = (\omega/c)\beta$. In this case, with $\phi_{jl} = \tan^{-1}(\epsilon_j k_{lz}/i\epsilon_l k_{jz})$ and $\psi(\beta) = 2(k_{1z}d_1 - \phi_{12} - \phi_{10})$, we find for the quantity $(d\psi)/(d\beta)$ the result

$$\frac{d\psi}{d\beta} = -2\left(\frac{\omega}{c}\right)^2 \frac{\beta}{k_{1z}} D_1(\beta), \tag{A1}$$

where

$$D_1(\beta) = \left(d_1 + i\epsilon_1\epsilon_2 \frac{k_{2z} - k_{1z}^2/k_{2z}}{\epsilon_1^2 k_{2z}^2 - \epsilon_2^2 k_{1z}^2} + i\epsilon_1\epsilon_0 \frac{k_{0z} - k_{1z}^2/k_{0z}}{\epsilon_1^2 k_{0z}^2 - \epsilon_0^2 k_{1z}^2}\right). \tag{A2}$$

An interface mode of the (free) layered structure consisting of the 2-1 and 1-0 boundaries consists in general of multiply reflected fields in medium 1 with k-vectors $\mathbf{k}_1$ and $\mathbf{k}_1'$ and outgoing fields in media 2 and 0 with k-vectors $\mathbf{k}_2$ and $\mathbf{k}_0$ as sketched in Fig. 4. The time averaged power flow carried in the mode along x

per unit length in the y direction is computed from the formula

$$P = \int_{-\infty}^{\infty} dz \langle \mathbf{S} \rangle \cdot \hat{x} = -\frac{c}{8\pi} \mathrm{Re} \int_{-\infty}^{\infty} dz E_z B_y^*, \qquad \text{(A3)}$$

where $\langle \mathbf{S} \rangle$ represents the time averaged Poynting vector. The power P is, therefore, the sum of the power per unit length associated with the mode fields in the three regions 0, 1, and 2 (in the absence of a 3–2 boundary).

By computing the mode fields in the three media subject to the boundary matching relations and the mode condition $\phi_{12} + \phi_{10} = k_{1z} d_1 - m\pi$ and performing the required integration, we obtain for P the general result

$$P = \frac{c}{8\pi} |a_1|^2 (\mathrm{Re}\beta) \exp(-2\,\mathrm{Im}\phi_{12} - 2\,\mathrm{Im}k_{1x}|\,|, \qquad \text{(A4)}$$

where a_1 is the amplitude of the plane wave field with k-vector $\mathbf{k}_1$ in medium 1, and the bracket is expressible in either of the forms

$$\begin{aligned}|\,| = {} & \frac{|\epsilon_1/\epsilon_2|}{(\mathrm{Im}k_{2z})} [\cosh(2\,\mathrm{Im}\phi_{12}) + \cos(2\,\mathrm{Re}\phi_{12})| \\ & + \frac{|\epsilon_1/\epsilon_0|}{(\mathrm{Im}k_{0z})} [\cosh(2\,\mathrm{Im}\phi_{10}) + \cos(2\,\mathrm{Re}\phi_{10})| \\ & + \frac{1}{(\mathrm{Re}k_{1z})} [\sin(2\,\mathrm{Re}\phi_{12}) + \sin(2\,\mathrm{Re}\phi_{10})| \\ & + \frac{1}{\mathrm{Im}k_{1z}} [\sinh(2\,\mathrm{Im}\phi_{12}) + \sinh(2\,\mathrm{Im}\phi_{10})| \end{aligned} \qquad \text{(A5)}$$

or

$$\begin{aligned}|\,| = {} & \frac{1}{2} \exp(2\,\mathrm{Im}\phi_{12} \left[\frac{|\epsilon_1/\epsilon_2|}{\mathrm{Im}k_{2z}} \left| 1 + \frac{1}{r_{12}} \right|^2 \right. \\ & + \frac{|\epsilon_1/\epsilon_0|}{\mathrm{Im}k_{0z}} |1 + r_{10}|^2 \exp(-2\,\mathrm{Im}k_{1z} d_1) \\ & + \frac{1}{i\,\mathrm{Re}k_{1z}} \left(\frac{1}{r_{12}} - \frac{1}{r_{12}^*} \right) + \frac{1}{i\,\mathrm{Re}k_{1z}} (r_{10}^* - r_{10}) \exp(-2\,\mathrm{Im}k_{1z} d_1) \\ & + \frac{1}{\mathrm{Im}k_{1z}} \left(1 - \frac{1}{|r_{12}|^2} \right) \\ & \left. - \frac{1}{\mathrm{Im}k_{1z}} (1 - |r_{10}|^2) \exp(-2\,\mathrm{Im}k_{1z} d_1) \right] . \end{aligned} \qquad \text{(A6)}$$

In the case of either a dissipationless surface-plasmon mode where $\mathrm{Im}\epsilon_j = 0$, $\mathrm{Im}\beta = 0$, $\mathrm{Re}k_{jz} = 0$, for $j = 0,1,2$ or a dissipationless guided wave mode where (for $j = 0,1,2$) $\mathrm{Im}\epsilon_j = 0$, $\mathrm{Im}\beta = 0$, $\mathrm{Re}k_{0z} = \mathrm{Re}k_{2z} = 0$, and $\mathrm{Im}k_{1z} = 0$, Eq. (A4) for P reduces to

$$P = \begin{cases} \dfrac{c}{4\pi} |a_1|^2 \exp(-2\,\mathrm{Im}\phi_{12}) \beta D_1(\beta) & \text{surface plasmon,} \\ \dfrac{c}{4\pi} |a_1|^2 \beta D_1(\beta) & \text{guided wave,} \end{cases} \qquad \text{(A7)}$$

The result (A7) is consistent with the result given in Ref. 1.

References

1. L. M. Brekhovshikh, *Waves in Layered Media* (Academic, New York, 1960); D. Marcuse, *Theory of Dielectric Optical Waveguides* (Academic, New York, 1974).
2. P. K. Tien and R. Ulrich, J. Opt. Soc. Am. **60**, 1325 (1970).
3. R. Ulrich, J. Opt. Soc. Am. **60**, 1337 (1970).
4. J. Schoenwald, E. Burstein, and J. M. Elson, Solid State Commun. **12**, 185 (1973); E. Santamato and F. DeMartini, Nuovo Cimento B **59**, 223 (1980).
5. H. J. Simon, D. E. Mitchell, and J. G. Watson, Am. J. Phys. **43**, 630 (1975).
6. M. Fukui, V. So, and R. Normandin, Phys. Status Solidi B **91**, K61 (1979); D. Sarid, Phys. Rev. Lett. **47**, 1927 (1981); A. E. Craig, G. A. Olson, and D. Sarid, Opt. Lett. **8**, 380 (1983); J. C. Quail, J. G. Rako, and H. J. Simon, Opt. Lett. **8**, 377 (1983).
7. J. E. Midwinter and F. Zernike, Appl. Phys. Lett. **16**, 198 (1970).
8. T. Tamir and H. L. Bertoni, J. Opt. Soc. Am. **61**, 1397 (1971).
9. W. P. Chen, G. Ritchie, and E. Burstein, Phys. Rev. Lett. **37**, 993 (1976).
10. A. Otto, Z. Phys. **216**, 398 (1968).
11. The same equation can be obtained by solution of the coupled equations (44)′ and (45)′ in region x where $\tilde{B}_3(x)$ has the constant value A.
12. For a complete lateral shift of the profile it is necessary that there be complete coupling of the incident radiation into the surface mode so that no specular reflection occurs at the trailing edge of the incident beam.

This work is supported by the National Science Foundation grant ECS-8120348, Defense Advanced Research Projects Agency grant N60530-83-C-0089, and the U.S. Air Force Office of Scientific Research (AFSC) and the U.S. Army Research Office.

Optics '83: A Report on Emerging Technologies

The 2nd Annual Report on Optics by the Optical Society of America's Technical Council profiles research findings from around the country.

Long-Range Surface-Plasmon Polaritons

The physics of surface-plasmon polaritons propagating on very thin metal films that are bounded by similar and semi-infinite dielectrics or semiconductors has been extensively studied in the past two years. The interest in these polaritons arose after it was discovered[1,2] that they are accompanied by large electric and magnetic fields that can serve as a vehicle for enhancing linear and nonlinear interactions. These polaritons consist of two modes that can be excited preferentially. One mode has a range *along* the metal film that increases as the metal film thickness on which it propagates decreases (Long-Range Surface-Plasmon, or SRSP). The other mode has the opposite property, namely, that this range decreases as the metal film thickness decreases (Short-Range Surface-Plasmon, or LRSP). The range of a mode is determined by the ratio of the power that is carried by the lossy metal film and by the lossless bounding media via the evanescent fields: For the LRSP (SRSP), as the metal film thickness decreases, the fraction of the power carried by the evanescent fields increases (decreases), resulting in an increase (decrease) in the range.[2]

The first experimental observation of the difference in the properties of these two modes was reported by Kovacs[3]. The first experimental tracing [4] of the theoretical dispersion curves[1], and the fit between the calculated and measured Lorentzian absorption curves[5] of these two modes were recently reported with film thicknesses ranging from 100 nm down to 10 nm.

There are several important interactions that can take advantage of the enhanced fields of the LRSP. For example, a recent calculation involving a single interface surface-plasmon polariton has revealed that it can have a propagation constant which depends on the optical power that it carries[6]. By considering the two-interface polaritons, these two theories[1,6] could now be merged. It was found that the LRSP indeed has an enhanced optical power dependence of its propagation constant[7,8]. We are currently working on experiments to observe bistability in a system which utilizes the LRSP propagating on thin metal films bounded by two InSb crystals.[9]

Second-harmonic generation

Another application of the enhancement in the optical fields that accompany the LRSP is second-harmonic generation. It has been calculated and observed experimentally that single-interface polaritons can give rise to an enhancement in second harmonic generation on total internal reflection[10]. One could now use two-interface polaritons and show theoretically that the LRSP will give an increase of more than two orders of magnitude in this enhancement[11]. The predicted increase in the enhancement of the second harmonic generation efficiency has been recently observed experimentally[12].

We expect that the LRSP will be found useful for other applications as well. Because of the ease with which thin metal films can be deposited on practically any substrate, these modes can be used to probe metal-dielectric interface properties such as roughness, or charge carrier properties in very thin metal films, for example. – **Dror Sarid**, Optical Sciences Center, University of Arizona.

References

1. Dror Sarid, Phys. Rev. Lett. *47*, 1927 (1981).

2. Dror Sarid, Robert T. Deck, Alan E. Craig, Robert. K. Hickernell, Ralph S. Jameson, and J. J. Fasano, Appl. Optics *21*, 3993 (1982).

3. G. J. Kovacs, *Optical Excitation of Surface-Plasmon Polaritons in Layered Media*, in Electromagnetic Surface Modes, Edited by A. D. Boardman, John Wiley and Sons N.Y. 1982.

4. A. E. Craig, G. A. Olson and Dror Sarid, Opt. Lett., *8*, 380 (1983).

5. J. C. Quail, J. G. Rako, and H. J. Simon, Opt. Lett. *8*, 377 (1983).

6. Dror Sarid, Appl. Phys. Lett. *39*, 889 (1981).

7. Dror Sarid, R. T. Deck, and J. J. Fasano, J. Opt. Soc. Am. *72*, 1345 (1982).

8. G. I. Stegeman, J. J. Burke, and D. G. Hall, Appl. Phys. Lett. *42*, 906 (1982).

9. D. A. B. Miller, S. Des Smith, and Colin T. Seaton, IEEE J. Quant. Elect. *QE-17*, 312 (1981).

10. H. J. Simon, R. E. Benner, and J. G. Rako, Opt. Comm. *23*, 245 (1977).

11. R. T. Deck and Dror Sarid, J. Opt. Soc. Am *72*, 1613 (1982).

12. J. C. Qail, J. G. Rako, H. J. Simon, and R. T. Deck, Phys. Rev. Lett. *25*, 1987 (1983).

Novel System for Coupling to Surface-Plasmon Polaritons

Alan E. Craig, Grieg A. Olson and Dror Sarid

University of Arizona, Optical Sciences Center

Tucson, Arizona 85721

ABSTRACT

A novel system for coupling to surface plasmon polaritons has been designed, fabricated and assembled. Microcomputer controlled electronics provide for accurate and repeatable angular positioning of the waveguide coupler with respect to the incident beam, and for precise angular registration of detector output signals. The optical components, combined with a retroreflecting spherical-surface coupling prism, give apertured control of the beam profile at the coupling interface.

INTRODUCTION

Prism couplers have been used extensively to provide evanescent field (frustrated total internal reflection) coupling to optical guided wave structures. A discussion of waveguide couplers has been presented by P. K. Tien[1]. Prism coupler systems usually comprise a triangular cross-sectioned prism of high refractive index glass mounted on a rotary table secured by one of a variety of clamping structures which also controls the proximity of the prism to the waveguide. Properly constructed clamping schemes can produce coupling efficiency as high as 94% [2,3]. The entire assembly is positioned so that the center of rotation of the table and the center of the prism-waveguide combination on the table lie in the path of a quasi-collimated beam of a laser. The table is rotated until the condition for coupling the incident light to the waveguide structure is satisfied.

To observe either the coupling efficiency or the angular width of the coupling regime, the power of the beam which is reflected from the coupling interface is monitored by a detector as a function of the angle of incidence. For a symmetrically shaped triangular prism, the reflected beam exits the prism at an angle relative to the coupling interface which is equal to the angle between the incident beam and the interface. Thus the angle between the incident and reflected beams is twice the angle separating the incident beam from the normal to the coupling interface. Rotating the prism causes the reflected beam direction to change at an angular rate twice that of the prism. A description of the propagation direction of the reflected beam for an asymmetric triangular prism requires a more complicated calculation. Arranging for this light to fall continuously on a detector as the table and prism waveguide structure

rotate is difficult with systems incorporating triangular prisms.

Triangular prism systems possess other undesirable optical characteristics. As the prism is rotated, the point where the incoming beam intersects the coupling interface walks along the interface. There is no axis around which the prism can be rotated to ensure that the beam always intersects the coupling interface at a fixed point. Unless the low refractive index gap region across which the light couples to the waveguide is perfectly uniform in thickness, this walking causes variation in the coupling efficiency. The efficiency is especially sensitive to gap thickness for coupling angles near the critical angle in the prism. Moreover, loss by reflection as the light enters the prism varies with angle of incidence, according to the Fresnel equations. These factors cause variations in the measured signal that are not characteristic of the guided mode, and for which compensation can be difficult or even impossible.

The system described below resolves many of the undesirable features of traditional prism coupler systems. In addition, it provides flexibility for controlling the beam's amplitude profile and transverse extent at its intersection with the coupling interface, which is particularly important when measuring the shape of the profile of the reflected beam.[4]

OPTICAL SYSTEM

A schematic of the optical system is shown in Fig. 1, and a photograph and sketch of the prism appear in Fig. 2. This prism is the keystone of the design.

The prism is made of a high index glass, SF56, having a refractive index at a wavelength of 632.8 nm of n=1.7788 (interpolated from Schott catalog data). Before

grinding the hemispherical surface, the glass block was polished flat on one side, sawed in half, mirror coated with aluminum on the polished sides, then cemented together with the mirrored sides in contact. Next, a base was polished perpendicular to the internal mirrored surface forming a retroreflecting corner. Then the hemispherical surface, centered on the intersection of the base with the internal mirrored surface was polished. The final radius of the hemisphere is 11.8 mm.

The micrometer pressing on the base of the prism controls the thickness of the low index gap across which the light couples to the waveguide. By adjusting this micrometer, the amount of light coupled to the mode can be varied. The coupling constant is given by[4]

$$h = \exp\left[-\left(k^2 - \frac{\epsilon_2 \omega^2}{c^2}\right)^{1/2} d_2\right], \qquad (1)$$

where k is the longitudinal component of the wave vector, c is the speed of light in vacuum, ω is the frequency of the light, ϵ_2 is the dielectric constant of the gap and d_2 is the thickness of the gap. In our system the coupling constant can be varied from 0 to 1/2.

The beam from the HeNe laser is incident on a spatial filter (a 3.8 mm focal length, infinite conjugate microscope objective with a 5 micron pinhole at its focal point), and an achromatic doublet lens collimates the light. An adjustable rectangular aperture and a beam splitter are located in the collimated space. A second achromatic doublet brings the beam to a focus at the front focal point of the spherically surfaced prism, whose base is the coupling interface. The spherical surface again collimates the light. The ray bundle will retroreflect, bouncing first off the internal, mirrored surface, then off the coupling surface (or perhaps in reverse order). These rays then traverse the hemisphere

again and are refracted to pass through the same focal point. Now rotating the prism about its polar axis (defined by the retroreflecting corner) causes the angle of incidence of the light bundle on the coupling interface to change by the same amount. Since the retroreflecting corner and the center of the hemisphere lie on this axis, the beam does not walk along the coupling interface except to the extent that its intersection width increases as a result of its incident obliquity. In addition, the reflected beam is always found in the same place and propagating in the same direction. Although curved surface prism couplers have been used by other researchers[5] this one is unique in that it utilizes a retroreflecting hemispherical design.

The rectangular aperture is located such that it is imaged by the second achromat and the spherical surface of the prism onto the coupling interface. The demagnification of these two elements is the ratio of their focal lengths, 1:2.65. In use, the aperture dimensions are generally about 4 mm square; the imaged dimensions are thus about 1.5 mm. Adjusting the aperture allows different portions of the beam to pass for sampling various regions of the coupling interface. Furthermore, the beam incident on the interface maintains its rectangular intensity profile. Care must be taken that the slit dimensions not be made too small, since the demagnification increases the divergence of the beam's angular spectrum.

The beam splitters direct half of the return beam from the prism coupler to two detectors. The first beam splitter also directs some of the light to a slit and a mirror used for angle calibration. Light passes through the slit to the mirror and off the substrate holding the waveguide. At a well defined angle, the light will return through the slit to reach the detectors. This angle then provides a reference from which other directions can be measured accurately. The calibration is reproducible to $\frac{1}{240}$ degree.

One might expect the spherical surface of the prism combined with the prism's high refractive index to introduce a severe amount of positive spherical aberration to the beam. This is not the case in our system, since we use a small aperture. Standard texts treat aberrations in detail. In our case, the spherical aberration is given by

$$W_{040} = \frac{1}{8} \frac{y^4 n'^2 (n'-1)}{r^3} . \qquad (2)$$

where y is the marginal ray height at the surface, n' is the index of refraction of the prism, and r is the radius of curvature of the surface. With y=1 mm, r=11.8 mm and n'=1.7788 a simple calculation shows that the aberration introduced is $W_{040} = 0.19$ μm (less than a third of a wavelength).

If this aberration is a problem, additional correcting elements may be added to the system. In particular, a negative meniscus lens may be inserted between the spatial filter and the collimating lens to introduce negative spherical aberration to the beam, exactly compensating for the aberration of the prism. The collimating lens must be repositioned to maintain good collimation, and adjusting the axial position of the meniscus lens changes the amount of aberration introduced. The aberration correction can then be checked by inserting a plane parallel plate shearing interferometer into the collimated beam to simultaneously measure the aberration in the incoming and outgoing beams. Since the prism is used in double pass, the aberrations in the incoming and outgoing beams have the same magnitude (but opposite sign) when the beam inside the prism is well corrected. The meniscus lens, however, introduces additional light scattering from flaws and dust on its surface; if beam uniformity is important then the interference produced by this scattered light may cause problems more severe than the spherical aberration. For this reason the aberration control was removed from our system.

ELECTRONIC SYSTEM

The rotation of the table which supports the hemispherical waveguide coupler, and the registration and recording of the detected light signal, are controlled via a microcomputer in conjunction with various accessory electronic instruments. A flow chart of the control chain is presented in Fig. 3.

One of the detectors is a wavelength-filter-compensated silicon photojunction detector operated in photoconductive mode. It is preceded by a narrow band wavelength filter which allows operation when the room lights are on without serious degradation of the signal-to-noise ratio. The detector and its preamplifier are sensitive to a wide range of incident power, from 0.01 μW to 1 mW. From the detector the signal passes through a preamplifier to a digital multimeter. The signal is then transmitted in digital form to the microcomputer by the DMM when it is queried.

The other detector is a CCD 1728 element linear image sensor positioned so that the coupling interface is imaged onto the detector. This enables one to examine the intensity profile of the reflected beam. A discussion of the purpose and use of the CCD array will be presented elsewhere.

Completing the control loop, the microcomputer addresses and instructs a controller unit which produces the required pulse signals to drive the rotary table, on which the waveguide coupler is mounted and centered, to the desired angular position. The table is driven by a worm gear mechanism and may be positioned repeatably to within 3 arc minutes cumulative accuracy and 0.2 arc minutes repeatibility, with an angular step size of $\frac{1}{4}$ arc minute (0.00417 degree).

APPLICATIONS AND RESULTS

Our coupling system has been used to probe surface plasmon polaritons on thin silver films[6,7], using the attenuated total reflection (ATR) approach. This type of resonance is associated with a light wave guided by a symmetrical refractive index structure consisting of dielectric, metal, and dielectric layers. The attenuation of the polariton along the metal film is reasonably low (in the range of 30 cm-1) and therefore its resonance is fairly narrow. The theoretical width of the resonance is 0.001 degree for a silver film 5 nm thick and a wavelength of 632.8 nm. For the tested films, as thin as 10 nm, the angular widths of the waveguide resonances have been as narrow as 20% of the angular resolution achievable by the optical system, allowing close qualitative analysis of the system's capabilities. A plot of the angular reflectance of a very narrow resonance (theoretical width, 0.012 degrees) produced by the system is shown in Fig. 4.

The rectangular delimiting of the beam's cross-section at the coupling interface is a vital part of the system's design. It facilitates analysis of the various loss components of the guided mode, which consist of absorption in the metal, roughness scattering and out-coupling to the prism.[4] However, it is also the apparent limiting feature of the optical system's performance. Diffraction from a rectangular aperture only 1.0 mm in extent produces a beam, at wavelength 632.8 nm, that has a diffraction angular spectrum of 0.044 degrees, FWHM. An observed resonance 0.4 degree wide showed diffraction ringing when the aperture width was reduced below 0.8 mm. (With this aperture width, the first zero of the sinc function of the angular spectrum is at 0.38 degrees.) This angular width is more than ten times the resolution of our rotary table.

The small effective aperture is the result of the demagnification ratio (1:2.65) of the last achromat and the hemispherical coupler. An increase in the optical angular resolution may be obtained by increasing the size of the adjustable rectangular aperture. This change also requires greater attention to control of the off-axis beam quality. Decreasing the focal length of the second achromat would also help but is not practical because of the extremely short focal length and high numerical aperture that would be required.

Although we have used the system for measuring the dispersion curves of surface plasmon polaritons propagating on very thin metal films, the system can be used for exciting and probing optical waveguides and other surface modes as well.

CONCLUSION

A hemispherical, retroreflecting, ATR waveguide coupler system has been implemented which exhibits several attractive features compared to traditional prism coupler systems. Its use in a microcomputer controlled system to measure narrow angular resonances has been demonstrated.

This work is supported by the Air Force Office of Scientific Research (AFSC), United States Air Force, and the Army Research Office, United States Army; by the National Science Foundation, NSF grant ECS-8244893; and by the Defense Advanced Research Projects Administration, DARPA grant N60530-83-C-0089.

REFERENCES

1. P. K. Tien, "Integrated optics and new wave phenomena in optical waveguides," Rev. Modern Phys. **49**, Number 2, p.361 (1977).

2. Dror Sarid, "High efficiency input-output prism waveguide coupler: an analysis," Appl. Opt. **18**, Number 17, p.2921 (1979).

3. Dror Sarid, Paul J. Cressman and Robert L. Holman, "High efficiency prism coupler for optical waveguides," Appl. Phys. Lett. **33**, Number 6, p. 514 (1978).

4. Robert T. Deck, Dror Sarid, Grieg A. Olson and M. J. Elson, "Coupling between finite electromagnetic beam and long-range surface-plasma mode," Appl. Opt. **22**, Number 21, p. 3397 (1983).

5. For example, Erwin Kretschmann, "Die bestimmung optischer konstanten von metallen durch anregung von oberflachenplasmaschwingungen," Z. Physik **241**, p. 313 (1971).

6. D. Sarid, "Long-Range Surface-Plasma Waves on Very Thin Metal Films," Phys. Rev. Let. **47**, Number 26, p. 1927 (1981).

7. Alan E. Craig, Grieg A. Olson and Dror Sarid, "Experimental observation of the long-range surface-plasmon polariton," Opt. Lett. **8**, Number 7, p.380 (1983).

FIGURE CAPTIONS

Fig. 1 Optical system layout: Support optics for retroreflecting hemispherical coupler.

Fig. 2 a) Photograph of the coupler with retroreflecting laser beam.

b) Sketch of an overhead view of the coupler.

Fig. 3 Flow chart of control electronics.

Fig. 4 System resolution of approximately 0.044 degree is apparent from this experimental trace of a narrow (0.012 degree, theoretically) surface-plasmon ATR resonance.

OPTICAL SYSTEM

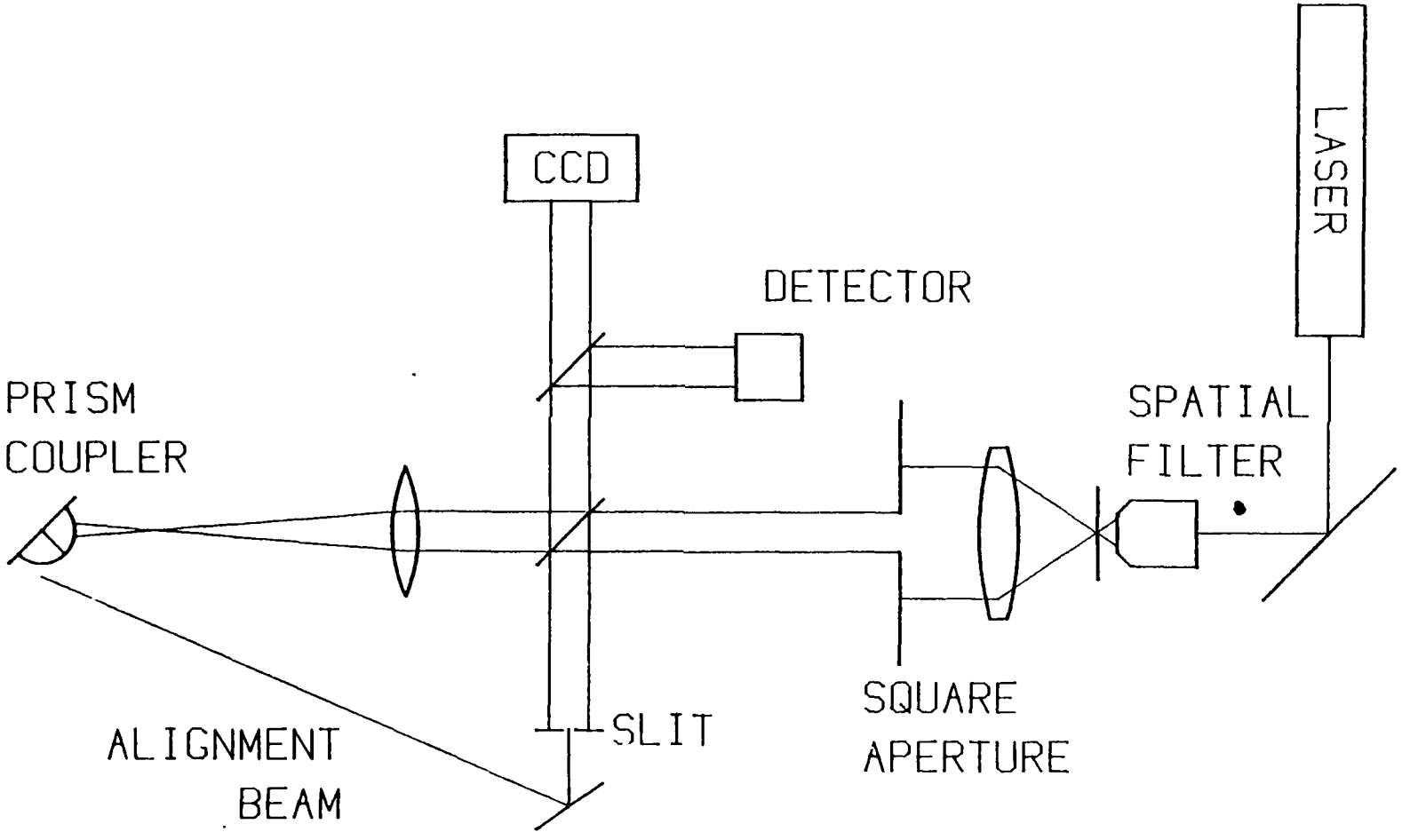

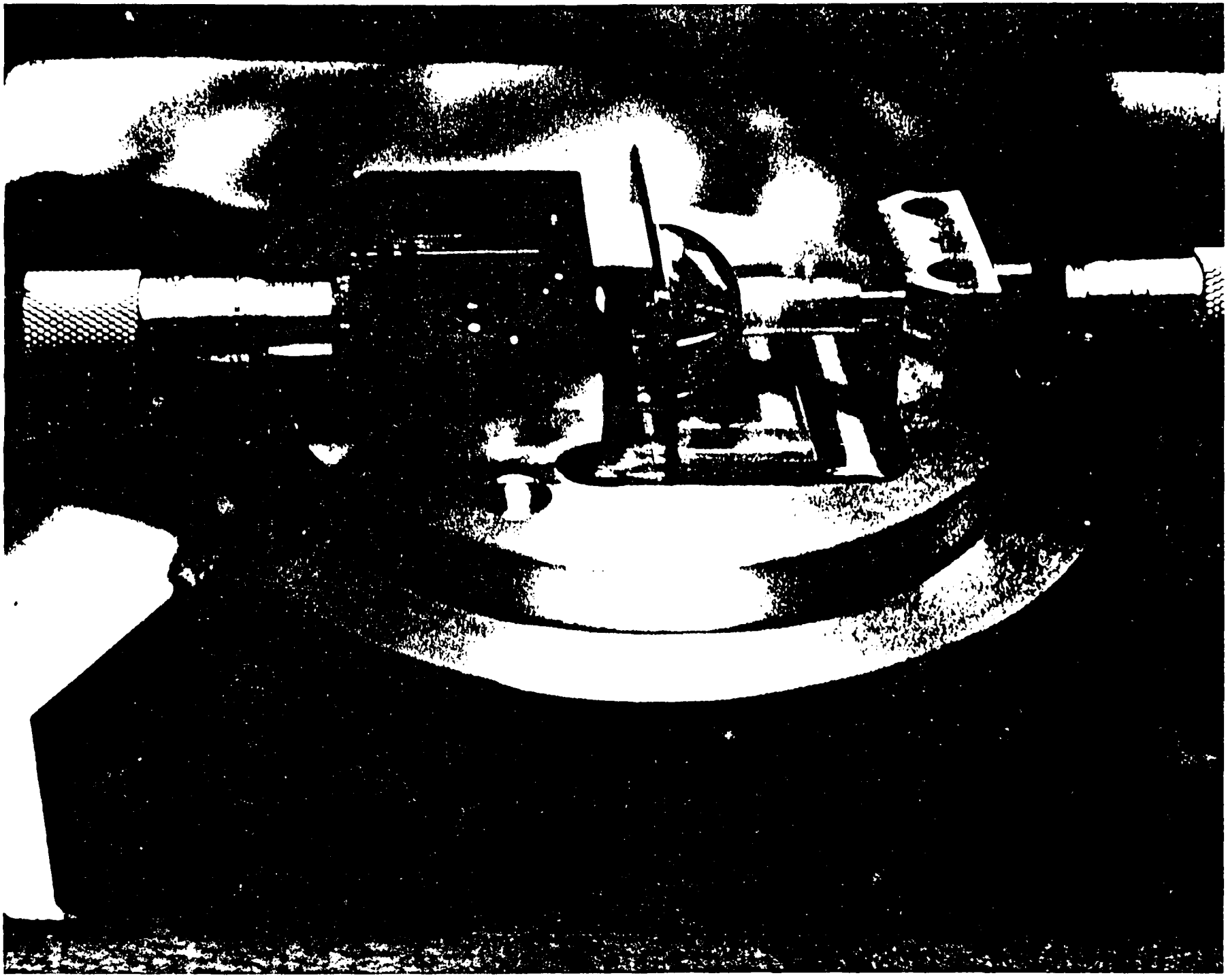

PRISM COUPLER

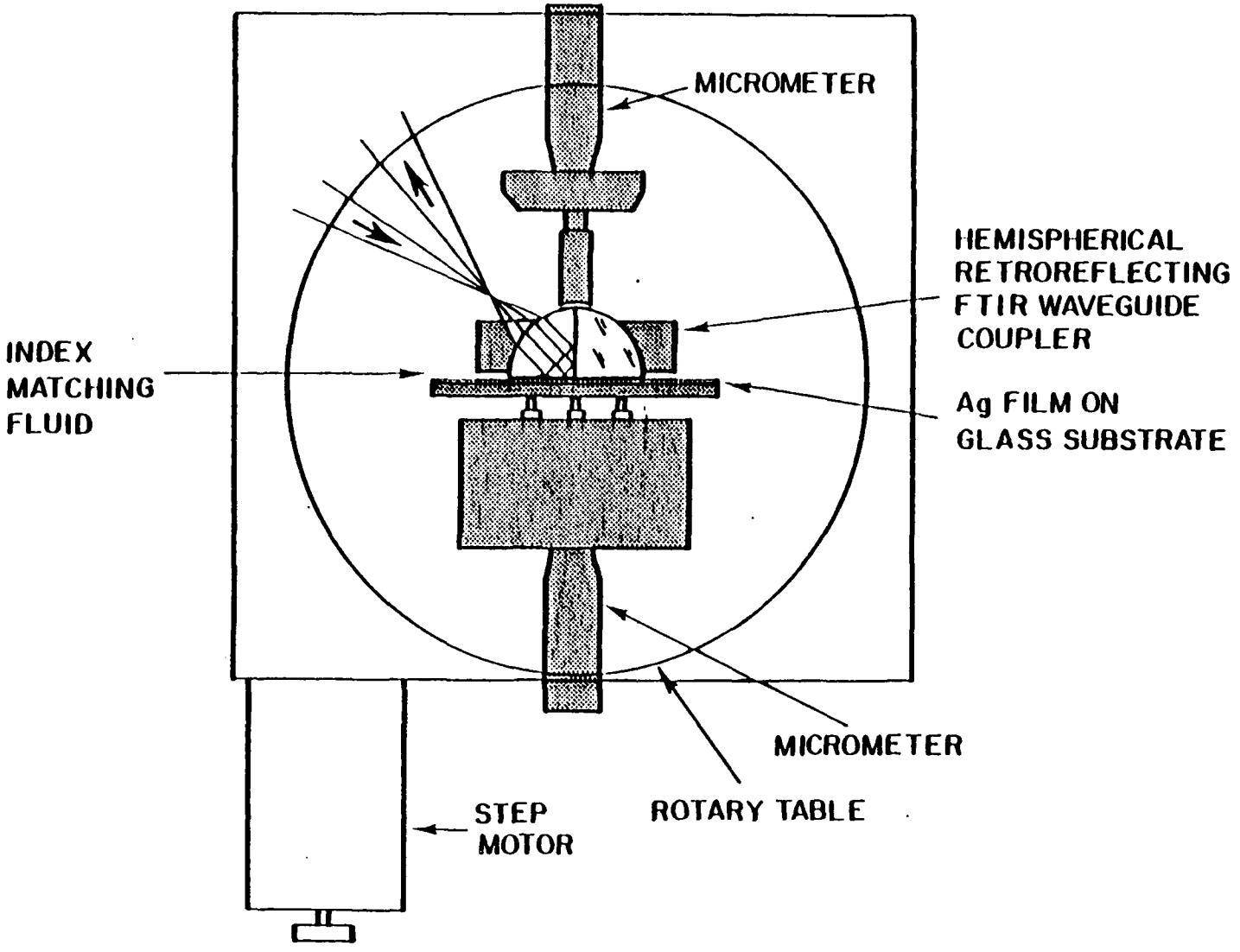

COMPUTER CONTROL

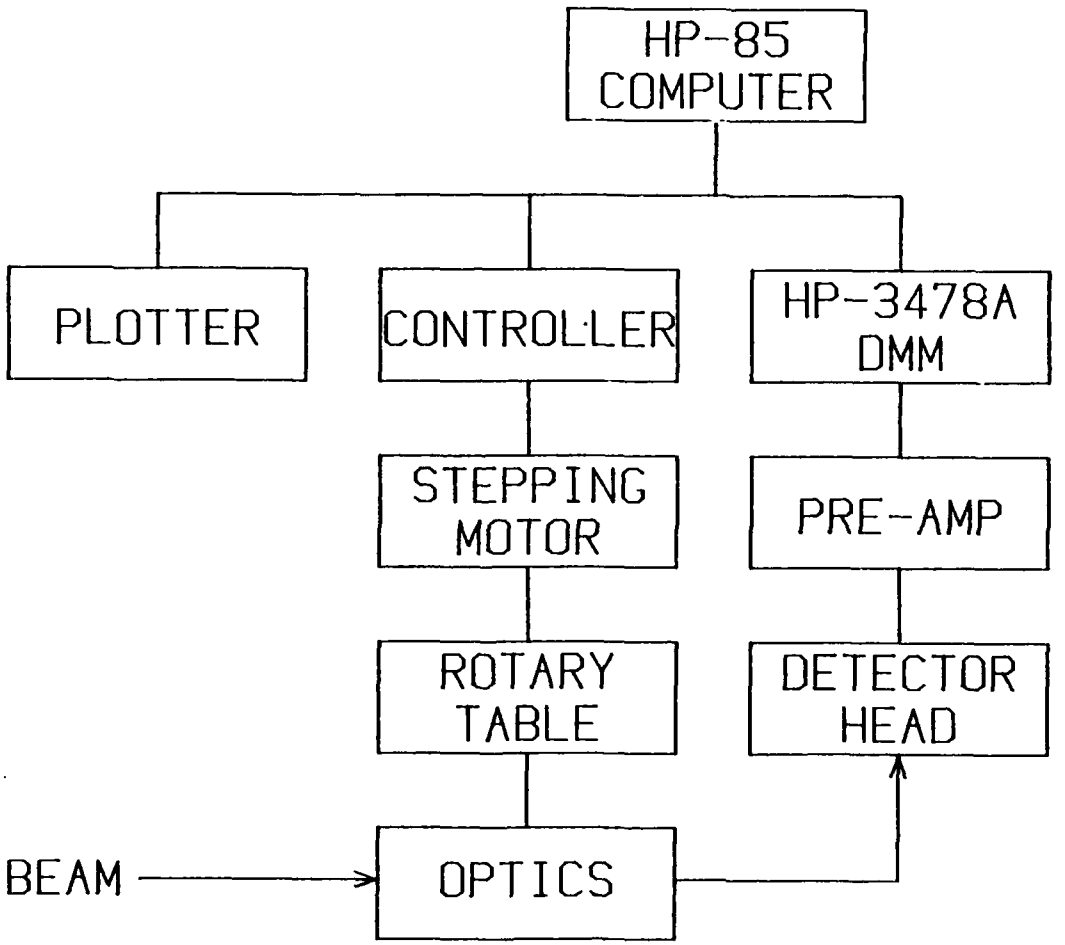

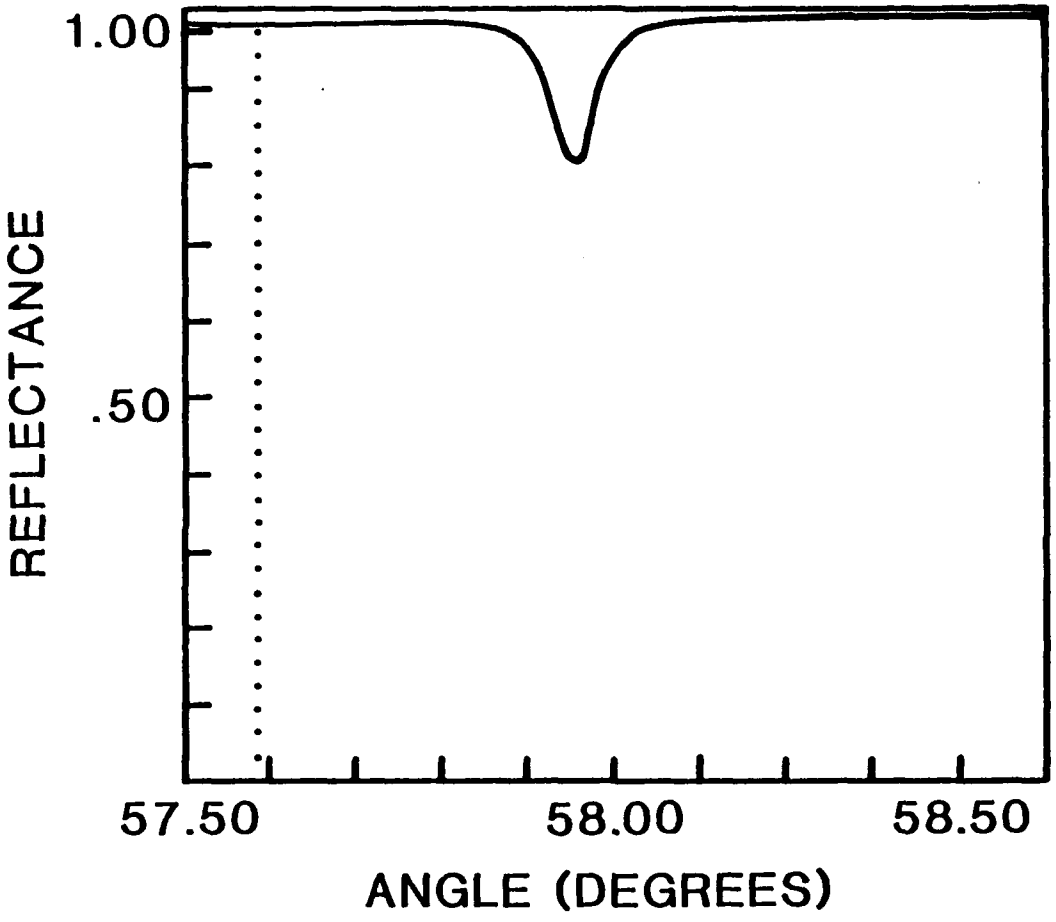
1.00
.50
REFLECTANCE
57.50
58.00
58.50
ANGLE (DEGREES)